2020-01-01

Early Detection of Asthma via Enhanced Resolution of Small Airways Using Ultra-Low Frequency Impulse Oscillometry

Christopher M. Aguilar
University of Texas at El Paso

EARLY DETECTION OF ASTHMA VIA ENHANCED RESOLUTION

OF SMALL AIRWAYS USING ULTRA-LOW FREQUENCY

IMPULSE OSCILLOMETRY

CHRISTOPHER MICHAEL AGUILAR

Doctoral Program in Electrical Engineering

APPROVED:

Rodrigo A. Romero, Ph.D., Chair

Erika G. Meraz, Ph.D.

Patricia Nava, Ph.D.

Sergio D. Cabrera, Ph.D.

Stephen L. Crites, Jr., Ph.D.
Dean of the Graduate School

To my beloved late father, Joaquin Aguilar, Jr.

EARLY DETECTION OF ASTHMA VIA ENHANCED RESOLUTION OF SMALL AIRWAYS USING ULTRA-LOW FREQUENCY IMPULSE OSCILLOMETRY

by

CHRISTOPHER MICHAEL AGUILAR, M.S.E., M.B.A.

DISSERTATION

Presented to the Faculty of the Graduate School of

The University of Texas at El Paso

in Partial Fulfillment

of the Requirements

for the Degree of

DOCTOR OF PHILOSOPHY

Department of Electrical and Computer Engineering

THE UNIVERSITY OF TEXAS AT EL PASO

May 2020

ACKNOWLEDGEMENTS

I would like to express my deepest gratitude and genuine respect for each member of my Dissertation Committee: Dr. Rodrigo Romero, Dr. Erika Meraz, Dr. Sergio Cabrera, and Dr. Patricia Nava. A finer quorum of not only distinguished professors, but also exceptional human beings, could have ever been assembled. Each member has made his/her own unique mark in my doctoral studies during my extraordinary experience at the University of Texas at El Paso and shall leave a lasting impression for life.

Special thanks must be given to my advisor and committee chairman, Dr. Romero, for his constant dedication and support throughout this entire process. I am grateful to have found such an exceptional mentor with tremendous insight and words of wisdom, which are forever committed to memory. Thank you very much for your trust, patience, guidance, and support. Very honorable mention must be made here as well to Dr. Meraz and her renowned work in Impulse Oscillometry and pediatric studies, which without your contribution my research would have not been possible.

I would also like to thank my former advisor, Dr. Homer Nazeran, for giving me the opportunity to conduct this research and for sharing his passion of biomedical devices, which has now become my own. His unwavering faith and optimism have been instrumental in my efforts.

To my mother, words cannot express my appreciation and love for you. Thank you for always believing in me, the years of helping me through life's lessons, and all the unselfish sacrifices made on behalf of myself and our family. You are mine and my sister's rock, forever.

This work is dedicated to the memory of my late father; the reason why I have committed my life to becoming as good of an engineer and father as he was. Dad, you set the bar very high.

Finally, to my girls JKL, thank you for taking this journey with me and offering me your beautiful smiles when I needed them most. I am eternally grateful to each of you. Te amo.

ABSTRACT

Examination of lung function for diagnosis and monitoring of diseases such as chronic obstructive pulmonary disease (COPD) and asthma can be performed with a variety of pulmonary function testing (PFT) techniques. The most commonly prescribed of these procedures are spirometry and whole-body plethysmography. However, these active participation tests depend on forced breathing maneuvers, may be physically exhausting, might not produce enough information, and are susceptible to being subject-dependent. In contrast, passive PFT approaches such as the forced oscillation technique (FOT) and the impulse oscillometry system (IOS) are increasingly being utilized for measuring lung mechanics because they require only minimal participation, which is a crucial advantage when dealing with very young pediatric patients, geriatric patients, and those with cognitive impairments or who are unconscious. Using external pressure oscillations superimposed onto tidal breathing, both FOT and IOS reveal intricate details behind breathing mechanics by measuring the frequency response of the respiratory system from the composite test signals to determine input impedance at the airway opening and detect lung obstructions and restrictions.

IOS features a unique discriminative property to identify the location of lung obstruction, which makes IOS very valuable for the detection and diagnosis of small airways disease (SAD), also known as small airways impairment (SAI), and impending asthma potentially long before their clinical manifestation. However, IOS measurements are coarse and there is also a need for studies with test functions in the low frequency range to determine the respiratory impedance of distant airways. Furthermore, particularly for preschoolers, current limitations of IOS include the lack of an international test standard; a lack of reference equations, parameter values, and identifiable SAD biomarkers; and a high probability of impedance distortion and biased

estimations due to signal interference from spontaneous breathing at low frequencies or upper airway shunting effects at high frequencies.

This dissertation aims at an enhanced IOS determination of the function of small airways via analysis of their frequency response to facilitate early SAD detection, which is considered a phenotype and likely childhood precursor for the pathogenesis of asthma. The ultimate goal of this research is to aid diagnosis and monitoring of asthma at an early stage, to treat and control the disease, and improve the quality of life of asthmatic individuals, particularly pediatric patients. This research introduces the development of a novel electrical model of the respiratory system to determine the mechanical impedance of peripheral airways using IOS-based data in the range from 5 Hz down to tidal breathing frequency, the ultra-low frequency range (ULF). The presented approach models the effects of noninvasive application of ULF excitation signals into the respiratory system to parameterize its frequency response below 5 Hz and ascertain sharper resolution of 7th to 19th generation airways.

TABLE OF CONTENTS

LIST OF TABLES

LIST OF FIGURES

CHAPTER 1: INTRODUCTION

Asthma is a chronic allergic disorder, wherein hyper-reactivity of the immune response to stimuli and airborne allergens triggers an inflammation of the bronchial tubes in the lungs, resulting in constricted airways and impaired breathing [2]. Depending on the severity and frequency of attacks, physiological distress symptoms range from dyspnea and diffused sibilant rhonchi to hypoxemia in extreme cases, thereby limiting physical activity and severely restricting quality of life. In 2018, asthma affected over 26.5 million Americans (339.4 million people globally) and was responsible for 420,000 deaths worldwide, or more than 1,000 per day [3, 4], predominantly among those inhabiting the developing world and almost all of which were preventable. It is estimated that one in twelve adults in the United States currently suffer from asthma, which coincidentally is the same statistic for prevalence among children in this country [2].

1.1 PROBLEM STATEMENT

In recent decades, the prevalence of pulmonary obstructive diseases has grown sharply among children, which has been attributed in part to an increase in atopic sensitization (e.g. genetic predisposition, urbanization trends, etc.) [2]. With the proliferation of lung disorders and diseases on the rise, examination of lung function for diagnosis and monitoring of respiratory diseases such as COPD and asthma becomes crucial. Current options among respiratory diagnostic and monitoring techniques include a variety of pulmonary function test (PFT) devices and procedures developed over the last 60 years [REFS]. The most commonly prescribed and well-established procedures are spirometry and whole-body plethysmography (WBP), which are often performed in tandem [1, 5]. In fact, spirometry is considered the PFT gold standard [5, 6] due in part to its

historically extensive body of knowledge and present adherence to a set of quality standards (adult-specific) established by the American Thoracic Society (ATS) and European Respiratory Society (ERS) [7, 8]. However, both spirometry and WBP are active participation tests that depend on extreme breathing maneuvers, may be physically exhausting, might not produce enough information, and are susceptible to being subject-dependent.

In contrast, passive PFT approaches such as the forced oscillation technique (FOT) and the impulse oscillometry system (IOS) are increasingly being utilized for measuring lung mechanics, though their historical rate of adoption has been lessened due to their atypical procedures, abstract parameters, and technical complexity. Researchers' and clinicians' increasing interest in FOT and IOS is mainly due to their distinctive ability to discriminate between central and peripheral lung obstruction. Additionally, these techniques require only submissive participation from the participant, which is a crucial advantage over other procedures when dealing with very young pediatric patients, geriatric patients, and those with cognitive impairments or unconscious.

Using external acoustic pressure waves superimposed onto spontaneous breathing, both FOT and IOS determine respiratory mechanics by measuring the relation between pressure waves applied and the resulting respiratory airflow at the mouth. The resulting respiratory system input impedance response, Z_{rs}, is used to detect lung obstructions and assess their degree of severity.

Application of these passive PFTs, via demonstration of their related fundamental principles of operation with respect to their measurements of Z_{rs}, primarily focuses on their extent of use in identifying central versus peripheral discriminative features, given that both techniques enable a detailed and accurate observation of lung mechanics for the potential identification of obstructions and pathologies in the respiratory system. Considerable research and clinical work still must be performed to leverage IOS capabilities to scrutinize small airways and alveoli utilizing

ultra-low frequencies (ULF) in search of reliable precursors and antecedent indicators for early detection of respiratory diseases, i.e. asthma. In addition, respiratory system models must be developed or extended into the ULF range to support research and clinical practice targeting small airway disease.

1.2 Small Airway Disease and Obstructive Pulmonary Disorders

Small airways disease (SAD) refers to the obstruction, inflammation, fibrosis and remodeling of the small airways. SAD may underlie asthma persistence, as most standard inhaled pharmaceutical treatments are unlikely to penetrate into pulmonary peripheral regions, but instead mainly therapeutically affect the large, central airways [33].

Chronic obstructive pulmonary disease (COPD) refers to an inflammatory disorder provoking airflow blockage, dyspnea, productive cough, and diffuse sibilant rhonchi. Frequent and prolonged exposure to irritants and allergens is the main source of this disease [1]. COPD is often considered to include a group of related and contributory respiratory disorders, primarily encompassing bronchitis and emphysema, typically occurring together but varying in severity. Bronchitis is characterized by inflammation of the lining of bronchial tubes that branch from the trachea, while emphysema can be described as a progressive disease causing dyspnea due to over-inflation of alveoli.

Bronchiectasis is another obstructive pulmonary disease, although functionally different from previously described diseases, with symptoms including productive cough and recurrent respiratory infections. Symptoms are produced and exacerbated by pathological dilation of airways, which in turn prevents ciliary transport of sputum out of the airways thus allowing these secretions to remain in the smaller airways cultivating bacteria.

Lastly, asthma is a very prolific and precarious respiratory disorder characterized by inflammation and constriction of the airways that causes a severe reduction in airflow. Marked by the overstimulation of the immune response and accompanying production of excess sputum, acute episodes can occur followed by extended symptom-free periods.

All of the conditions just mentioned result in either some type of not fully- or irreversible damage occurring in the lungs. Therefore, early screening for the recognition of accelerated and progressive deterioration of the small airways via sensitive PFT may provide awareness for a predisposed development of asthma and therefore allow timely and systemic intervention before the onset of chronic airflow obstruction and further lung function decline, commonly associated with COPD and this morbidity.

1.3 Clinical Relevance and Significance of the Problem

Research shows a unique discriminative property of IOS to identify the site of airway obstructions, which makes IOS very valuable for the detection and diagnosis of SAD and impending asthma, potentially long before their clinical manifestation. However, IOS measurements are coarse and typically limited to frequencies well above the tidal breathing frequency. To probe the small airways, IOS measurements must be extended to the ultra-low frequency range (ULF), i.e. below 5 Hz, for a more sensitive and specific determination of peripheral respiratory impedance in the quiet zone. Collectively the small airways compose a significantly large portion of the lungs' volume and surface area in comparison to the central airways, yet account for only 10 percent of total airway impedance [9], making this peripheral zone contribution more challenging to detect. This research aims at extending IOS data and models into the ULF range to explore and determine whether they will offer increased sensitivity for

detection of peripheral obstructions in the lungs, which potentially predisposes the onset of small airway disease in suspect patients, and provide an earlier detection of asthma.

Furthermore, particularly for preschoolers and geriatric patients, current limitations of IOS include: the lack of an international test standard; a lack of reference equations, parameter values, and identifiable SAD biomarkers; and a high probability of impedance distortion and oscillatory signal interference due to tidal breathing and upper airway shunting effects. These effects become yet more complicated in early childhood subjects, where discernment between the effects of disease from the influences of growth and development is critical to clinical management [10]. PFT, however, offers opportunities for prevention, reversibility, and early identification of respiratory disease. For instance, both spirometry and IOS can identify airflow obstruction before COPD symptoms emerge and five to ten years before any signs may surface on X-ray images [6].

1.4 Research Objectives and Proposed Solution

Significant advantages of IOS over other PFTs in clinical practice and research include its objectivity, high sensitivity for the detection of SAD, improved time resolution of measurements, and subject passive participation. In current clinical practice, however, IOS complex test results lack comprehensive and discriminative respiratory impedance data below the standard 5 to 30 Hz range where it has been suggested that results are most sensitive to normal physical processes and pathologic structural alterations [11], especially in small airways. Given that most of data and current practice do not encompass ultra-low frequency measurements of respiratory system impedance, which correlate directly with the condition of the small airways, the research questions guiding this work are, first, can existing IOS data be validly expanded into the ULF range for SAD studies? And, second, how can electrical pulmonary system models be developed, extended, or

tuned into the ULF range to reveal specific information about the condition of small airways based on IOS PFT to support research and clinical practice targeting SAD?

Hence, the aim here is to describe the calculated research approach used to address the challenges in applying composite ULF test signals and extracting valid respiratory impedance measurements from the frequency response of the small airways, analyzing the results, and modeling the outcomes. For the sake of this research and for future reference, ultra-low frequency (ULF) is defined as all signal frequencies from $0+\varepsilon$ to 5 Hz, for $\varepsilon > 0$ and $\varepsilon \rightarrow 0$, which includes the spontaneous tidal breathing frequency.

The main focus of this research is the evaluation of ULF IOS data and electrical models with the following goals:

Objective 1: To develop and optimize an electrical analog, lumped parameter SAD model to characterize the impedance response of the human respiratory system subject to test under ULF IOS.

Objective 2: To design a model parameter estimation algorithm to define optimal parameter values for a SAD electrical analog via regression analysis of IOS respiratory impedance measurements from an existing patient database.

Objective 3: To simulate the application of synthetic ULF test signals superimposed onto a tidal breathing signal and extract high quality respiratory system impedance outputs from an electrical IOS circuit model with optimized parameter values to detect evidence of SAD.

Objective 4: To quantitatively evaluate performance of the frequency response signals, primarily respiratory system impedance (Z_{rs}), and gauge the precision of transduced IOS circuit model parameter estimates via the coherence function (γ^2) and signal-to-noise ratio (SNR) to evaluate their effectiveness.

Objective 5: To assess the impact of simulated impedance of the respiratory system (Z_{rs} via SAD inverse and forward model approaches) and SAD-related model parameter estimates across the low-frequency range of interest for the subsequent identification of sensitive changes in respiratory system frequency response in comparison to competitive models and predetermined IOS indices from a patient database.

Research performed aims to enhance IOS sensitivity of small airway impedance characteristics via modeled ULF frequency response for reliable extraction of discriminative predictor features of SAD. A key deliverable of this research is the development of a novel electrical analog of a SAD respiratory model that circumvents the standard test range and instead concentrates on the unfamiliar ULF range. Circuit simulations, nonlinear regression with extrapolations, and statistical analysis using clinical parametric data from a 2006 IOS study of 112 children ages 5 to 17 are performed to assess the validity and accuracy of the ULF SAD model, especially in pediatric patients.

CHAPTER 2: LITERATURE REVIEW

The mechanical properties of the respiratory system become explicitly important when the normal rhythm of breathing becomes compromised. Researchers and clinicians rely on the measurement of these properties to determine the conditions of lung function and reach a diagnosis [39]. The objective of this chapter is to offer an overview of PFT to analyze the manner in which mechanical properties of the lung have been measured, modeled, and researched.

2.1. PHYSIOLOGICAL INTERPRETATIONS OF RESPIRATORY IMPEDANCE

Pulmonary function tests measure a set of system parameters that serve as key indicators of the current state of the lungs. These indicators are interpreted to diagnose, monitor, and treat respiratory disorders via a combination of expertise in the field and comparison against established references including test standards, equations, and threshold values.

The principal parameter that only IOS and FOT can measure directly via external pressure oscillations is respiratory system impedance (Z_{rs}). This parameter may be defined as the mechanical load of the respiratory system to ventilation, or in IOS/FOT terms, the sum of all forces in the airways and surrounding parenchyma that oppose the injection of the pressure oscillation down into the lungs [39]. Such forces include frictional loss in the airways, or resistance, plus gas inertive and tissue compliance influences, or reactance. By definition, the sum of respiratory system resistance (R_{rs}) and reactance (X_{rs}) produces the total respiratory system impedance (Z_{rs}).

From the IOS/FOT perspective, Z_{rs} is the mechanical response to the respiratory system to an acoustical pressure wave traveling from the airway opening through the trachea and ultimately to the alveoli. The airflow induced by this pressure wave will be impeded in a non-

uniform fashion by the Venturi effect in the airways and shunting properties of the distended parenchyma [37]. Z_{rs} is comprised of R_{rs}, which represents the energy dissipation caused primarily by flow drag against the viscous walls of the narrow airways, and X_{rs}, which is considered as energy storage that is relative to a tissue's elasticity or compliance, its inverse.

2.1 THEORETICAL FOUNDATIONS OF FOT AND IOS

The pulmonary testing scheme of applying forced oscillations, primarily via sinusoidal air pressure fluctuations at the mouth or around the chest, to ascertain flow response of the lungs and thus determine the state of respiratory mechanics in humans was first researched by DuBois *et al*. (1956). Pressure and flow measurements are ascertained by the instrument's pneumotach (airflow meter) and pressure transducer (scales and digitizes an acoustic signal to a voltage output reading), respectively. The acquisition of this FOT flow response for subsequent computation of mechanical lung impedance provides a method for detection of SAD and monitoring of asthma. Since its introduction, FOT has been a replacement or an adjunct to spirometry when the focus of study is on small airways, which are the predominant site of airflow obstruction in asthmatics [12].

Instead of relying on total lung capacity (TLC) and residual volume (RV) measurements as proxies for the calculation of respiratory impedance as done in spirometry, FOT utilizes mechanical perturbations, i.e., external pressure signals, superimposed over normal breathing to derive any underlying level of obstruction. A loudspeaker or an air piston are common sources of acoustic pressure signals to be applied at the airway opening. The input impedance of the respiratory system (Z_{rs}) can be approximated from the ratio of the fast Fourier transform (FFT) of the FOT pressure input to flow response at each test frequency. Z_{rs} represents the impedance of

the whole respiratory system comprised of both resistance (R_{rs}), or frictional loss, and reactance (X_{rs}), or elastic and inertial load, and it can be expressed as the complex quantity

$$Z_{rs} = R_{rs} + iX_{rs}, \text{where } i = \sqrt{-1}. \quad (2\text{-}1)$$

R_{rs} describes the dissipative mechanical properties of the respiratory system and encompasses the resistance of central and peripheral airways, lung tissue, and chest wall. Since the resistance contribution from the latter two is typically negligible, R_{rs} is predominantly determined by caliber, wall surface, and structure of the airways. X_{rs} describes the energy storage capacity of the respiratory system and represents the mass-inertive forces of the moving air column in the conducting airways expressed in terms of frequency-dependent capacitance and inertance [13].

FOT can reliably discriminate between large and small airway obstruction via high versus low frequency response characteristics, respectively. The FOT high-frequency response (>20 Hz) is determined by proximal airways, whereas its low frequency response (<15 Hz) is determined by small airways. FOT parameters, where P_f stands for measured parameter P using a test signal with the fundamental or reference frequency f, including R_5, R_{20}, X_5, X_{20}, and resonant frequency, F_{res}, indicate the relationship between impedance measurements, site of airflow deficiency, and the degree of obstruction, as pulmonary impedance varies inversely with the caliber of airways [14]. Reference to these specific FOT parameters may support the diagnosis of a pulmonary obstructive disease such as bronchitis, emphysema, bronchiectasis, and similar dysfunctions. Additionally, the frequency dependence of resistance (fdR = $R_5 - R_{20}$) can be used as another indicator in determining whether an obstruction is present in large versus small airways. A distinctive feature of SAD is a relatively high fdR, which is indicative of higher resistance within the lumen of peripheral airways. Thus, impairment causes can be identified as follows [10]:

1. High R_{20} implies proximal airway obstruction.

2. High R_5 and $|X_5|$, where |a| indicates absolute value, imply peripheral airway obstruction, e.g. asthma.
3. High fdR implies small airways disease.

FOT shares physical, anatomical, and physiological bases with IOS [15]. However, the former uses as test signals a mono-frequency sine wave sequence or pseudorandom noise (PRN) [16, 17], whereas the latter uses mixed multi-frequency (5 – 30 Hz) impulse signals. Using conventional equipment, these IOS input pressure pulses may be applied at up to 10 impulses per second, thereby allowing for the reliable analysis of intra-breath variation in impedance, comparable to FOT. However, IOS applications, as in this research, typically utilize 5 impulses per second to record longer respiratory time constants (τ) that usually provide more information and evidence of respiratory defects [13].

IOS uses spectral analysis of the pressure (P_{rs}) to flow (V'_{rs}) ratio at the mouth to calculate Z_{rs} in the test signal frequency range to determine the location and extent of any airway obstructions, with respiratory system impedance routinely calculated at the desired frequency via FFT and represented in acoustical terms in the frequency domain as follows:

$$Z_{rs}(f) = P_{rs}(f)/V'_{rs}(f), \text{where } \{0 < f \leq f_{max}\}. \quad (2\text{-}2)$$

IOS is advantageous for diagnostic use in pediatric and geriatric cases because only brief, passive subject cooperation is necessary. For detection of SAD, IOS compares favorably to other methods including spirometry, WBP, and gas dilution techniques that lack the required sensitivity to detect abnormalities and measure airflow obstruction in peripheral bronchi [1]. To identify SAD, IOS is also better than chest radiographs because of their inadequate spatial resolution and interpretation-dependent accuracy [18].

IOS data analysis is based on electrical and mathematical models of pulmonary function in terms of impedance, which is potentially a more robust method. Yet, visualizing and relating these concepts to biomechanical or physiological analogs may still prove nontrivial and even counterintuitive. As an example, Fig. 2.1 presents a common approach for visualization of respiratory system resistance and reactance using arithmetic mean values per group of healthy, pre-SAI, SAI, and asthmatic subjects for discrete test frequencies commonly used in research and clinical practice. Notice that small airway impairment (SAI) is another way to refer to small airway disease (SAD).

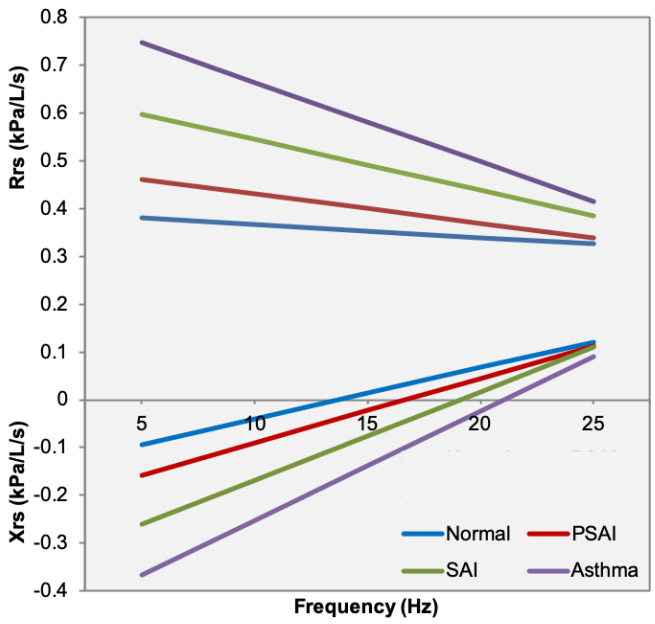

Figure 2.1: Respiratory system impedance response as a bivariate linear regressions of respiratory resistance (R_{rs}, four top responses) and reactance (X_{rs}, four bottom responses) versus applied impulse signal frequency. Input data obtained from children ages 5-17 [12]. Severity of pulmonary obstruction is indicated in trend lines via higher resistance and lower reactance, particularly at 5 Hz. Lines indicate Normal (healthy), small airway impairment (SAI), pre-SAI, and Asthma IOS results.

2.2 IOS Background and State-of-the-Art Noninvasive PFT

Measurements of the mechanical properties of the respiratory system depend heavily on the PFT technique used to acquire them, as shown in tables 2.1 and 2.2. A challenge here is that

lung disease resemblances and symptomatic crossovers among distinct yet similar conditions blur traditional delineations for detection of obstructions. Thus, it is important to consider the evolution of techniques and what they offer to estimate or measure respiratory parameters of interest to determine diseases or impairments. Moreover, analysis and interpretation of PFT results are often compared against established, yet limited, sets of demographic- and/or anthropometric-specific reference values, thereby making the choice of PFT critical. In addition, various algorithms may be used to classify subjects as either healthy or impaired and to assess degree of dysfunction and even therapeutic response under provocation testing.

Although its tests do not directly measure respiratory resistance, spirometry is the de-facto PFT of choice for detecting airflow limitation and increased resistance via peak expiratory flow (PEF) and forced expiratory volume in t seconds (FEV_1), respectively [19]. For noninvasive detection of SAD, which spirometry cannot measure directly, both FOT and IOS are better.

Since its inception circa 1956, as shown in Fig. 2.2, FOT eventually evolved in the mid-1970's into IOS, which uses mixed multi-frequency (~5 to 30 Hz) acoustic impulses as input test signals, versus the single-frequency sine wave signal approach used in fundamental FOT or the pseudorandom (PRN) signals used in auxiliary FOT techniques [16, 17]. IOS was later commercialized in 1993 by Jaeger [15]. Fig. 2.2 shows a timeline of the evolution of FOT/IOS.

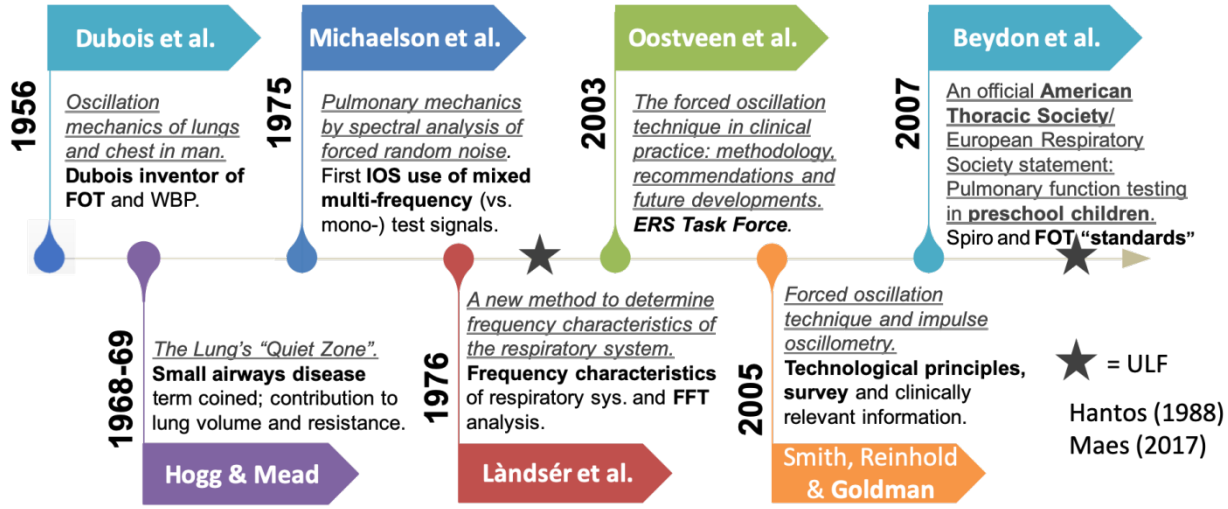

Figure 2.2: Historical development of FOT and IOS.

Tables 2.1 and 2.2 present a comprehensive analysis of current noninvasive PFT methods and equipment, with an emphasis on device physics. These tables also include assessments such as discrimination of disease and site of impairment; clinical applications; and reference populations best served by each technique. The top eight PFT techniques considered are listed in order of utilization frequency or impact level. Methods linked by the same physics are shaded with the same color; methods include: 1) flow-volume mechanics, 2) oscillometric impedance response, and 3) airway occlusion resistance. Parameters listed in the tables were selected based on relevance and how well their measurement ranges correlate. Assessments of airway responsiveness to bronchodilators or bronchoconstrictors and use of gases other than air are not included in the analysis.

Table 2.1: PFTs based on flow-volume mechanics or airflow interruption.

PARAMETER	SPIROMETRY	BODY PLETHYSMOGRAPHY	INTERRUPTER	AIRFLOW PERTURBATION (APD)
Measurement Principle	Measures relative lung volumes and air speed upon forced maneuvers to describe respiratory mechanics in time domain	Measures absolute lung volume via pressure or flow change (Boyle's Law) caused by chest movements inside airtight box	Rapid Airway Occlusion Maneuver by Valve/Shutter wherein mouth pressure equilibriates w/ alveolar pressure	Partially obstructs airflow during tidal breathing to measure only respiratory resistance in time domain
Key Parameters	Volumes: FEV1, FVC; Flows: PEFR, FEF25–75%	FRC, sRaw, Raw, TLC, RV, TGV	Rint	Ravg = (Rin + Rex)/2
Device Type	Spirometer	Cabin with sensors to measure box and mouth pressure	Pneumotach w/ pressure transducer; shutter in series	Smalll, Portable, Lightweight, Quick and Inexpensive
External Excitation Wave Generator	N/A	N/A	N/A	Rotating segmented wheel w/ open and screened segments
Single or Multiple Test Signal Frequencies	N/A	N/A	N/A	Single - One Wheel Speed
Input Test Signal and Typical Frequency Range	N/A	~ 1-4 Hz Panting Frequency	Airflow Interruption every 80-100 ms (10-12.5 Hz)	2 Pertubations per Wheel Rotation (6.7-9.8 Hz)
Patient Cooperation Req./ Breathing Maneuver	Active / Forced Exhalation and Deep Inhalation	Tidal Breathing / Panting / Forced In-, Ex-halation / Shutter Maneuver	Minimal Cooperation; Passive / Tidal Breathing	Minimal Cooperation; Passive / Tidal Breathing
Typ. Measurement Duration and No. of Repetitions	15 mins; 3 reps (2 highest results taken, 8 rep Limit)	2 mins; 3 reps	5-10 reps	60 sec; 3 reps
Tracks Real-Time Within-Breath Changes of Rrs_Zrs?	N/A; Flow-Volume Loop and Volume-Time Plot Track Inspiratory/Expiratory Cycles	N/A	Yes - Distinguishes between Rint-in v. Rint-ex	Yes - Distinguishes between Rin v. Rex
Discriminates Between Large & Small Airways Obstruction?	No - Primarily Measures Bulk Flow in Large Airways; SAD Mildly Correlates to FEF25-75%	No - High Sensitivity in Raw to Changes in Airway Caliber via Bronchoprovacation Challenge	No - Measures Only Total Inspiratory Resistance	No - Identifies upper airway disorders; Study of SAD correlation is unprecedented
Quality Control Indices for Data Integrity	No - Std. Test Method by ATS, yet Dependent on Cooperation	No - Basic Routine System Pressure and Vol Calibrations	Yes - Intraclass Correlation Coefficient (ICC)	No - Calibration via Mechanical Respiratory Analog

Table 2.2: PFTs based on application of oscillatory test signals.

PARAMETER	FORCED OSCILLATION (FOT or MFO)	IMPULSE OSCILLOMETRY (IOS)	HEAD GENERATOR (HGT)	AIRWAVE OSCILLOMETRY (AOS)
Measurement Principle	Measures pulmonary impedance, Zrs, via pressure and flow (oscillations) at the mouth during spontaneous breathing	Similar to FOT except uses mixed multi-frequency test signals and FFT to calculate impedance (Zrs = Rrs + Xrs)	Same as FOT except test signal applied to a chamber enclosing the head to minimize upper airway shunt	Same as FOT except uses vibrating mesh as source of excitatory input test signal
Key Parameters	Zrs, Rrs, Xrs, Fres, fdR, Ax	Zrs, Rrs, Xrs, Fres, fdR, Ax	Zrs, Rrs, Xrs, Fres, fdR, Ax	Rrs, Xrs, Fres, AX, Xin-ex, Vtidal, Respiratory Rate (RR)
Device Type	FOT Apparatus using Linear Regression Algorithm	Impulse Oscillometry System using Fast Fourier Transform	FOT Apparatus incl. 35-40L Chamber (e.g. Pulmosfor)	Portable, Handheld for use with Tablet/Laptop (e.g. tremoFlo)
External Excitation Wave Generator	Loudspeaker or Piston Pump (applied at mouth)	Loudspeaker (applied at mouth)	Loudspeaker (applied at canopy around the head)	Breathe-through Vibrating Mesh
Single or Multiple Test Signal Frequencies	Single or Multiple Discrete Freq. (sequentially applied)	Multiple	Multiple	Multiple - Non-harmonic 9- or 10-Frequency Composite Signal
Input Test Signal and Typical Frequency Range	Sine Wave (approx. 5-35 Hz) or Pseudorandom Noise	Square Wave Impulses (5-35 Hz; typ. every 5 Hz harmonic)	Pseudorandom Noise (4-30 Hz, every 2 Hz harmonic)	Pseudorandom Noise (Adult: 5-37 Hz; Pediatric: 7-41 Hz)
Patient Cooperation Req./ Breathing Maneuver	Minimal Cooperation; Passive / Tidal Breathing	Minimal Cooperation; Passive / Tidal Breathing	Minimal Cooperation; Passive / Tidal Breathing	Minimal Cooperation; Passive / Tidal Breathing
Typ. Measurement Duration and No. of Repetitions	8-16 sec; 3-5 reps	30 sec; 3-5 reps	16 sec; avg. of 2 to 3+ reps	20 sec; 3 reps
Tracks Real-Time Within-Breath Changes of Rrs_Zrs?	Yes - Based on Period of Excitation Signal w.r.t. Breath Duration; typ. ~Mean of Whole Val	Yes - Based on Period of Excitation Signal w.r.t. Breath Duration; typ. ~Mean of Whole Val	Yes - Based on Period of Excitation Signal w.r.t. Breath Duration; typ. ~Mean of Whole Val	Yes - Between Low Frequency Inspiratory & Expiratory Reactance
Discriminates Between Large & Small Airways Obstruction?	Yes - High Sensitivity via fdR (Central v. Peripheral)	Yes - High Sensitivity via fdR (Central v. Peripheral)	Yes - High Sensitivity via fdR (Central v. Peripheral)	Yes - High Sensitivity via fdR (Central v. Peripheral)
Quality Control Indices for Data Integrity	Yes - Coherence; Coefficient of Determination (Model Fit)	Yes - Coherence: an Index of Signal-to-Noise Ratio	Yes - Coherence; Coefficient of Determination (Model Fit)	Yes - Coherence; Automatic artifact detection/exclusion

Despite the availability of a few international recommendations for some PFTs, there is a need for determining the extent of correlation of indices and parameters to support comparative analysis of results across multiple different techniques. Likewise, experimental variability in PFT measurements includes effects of artifacts due to swallowing, coughing, or airflow leaks. Consecutive trials and statistics are used to reduce the effects of variability [17]. The latter itself is a source of variability across methods, as sample size, test cycle duration, number of trials, and parameter statistics vary between PFT implementations. Measurements in children have additional sources of variability due to their anatomically small, hard-to-fit, still developing features, which according to most experts correlates closely with the subject's height but may be debated [12]. In this work, data variability in the used pediatric data set will be considered as a factor in ULF IOS modeling to support accurate diagnoses of pediatric respiratory disorders.

2.3 RELATED WORKS

This section presents the main existing electrical models of the respiratory system over the widely adopted frequency range between 5 Hz and 25 Hz and above. Then it discusses low-frequency FOT, and finishes by presenting the concept and importance of ultra-low frequency IOS. An important consideration when dealing with low frequency test signals below the 5 Hz threshold, to determine Z_{rs} in this frequency range, is the effect of tidal breathing in measurement and processing. Here the main goal is to eliminate undesirable breathing frequency noise and reveal Z_{rs} values associated with small airway pathologies. A few methods exist for accomplishing this objective, and with very accurate results, but these methods have mainly succeeded when applied to unconscious patients or using invasive measurement procedures [41]. An important aim of this work is the enhancement in measurement sensitivity of IOS in the low frequency range to improve

localization of site and degree of obstruction. In turn, this higher resolution examination of Z_{rs} below 5 Hz may lead to timelier, more accurate detection and treatment of distal obstructive diseases such as SAD and asthma.

2.3.1 RESPIRATORY IMPEDANCE MODELING VIA ELECTRICAL ANALOGS

Human respiratory system analogs based on either a mechanical or electrical system modeling provide means to estimate and interpret IOS parameters. In this dissertation, only electrical models will be considered. Models investigated consist of Resistance-Inductance-Capacitance (*RIC*) circuits of various single- or dual-compartment designs, primarily of parallel component configurations shown in Fig. 2.3. A hierarchy of historical models established circa 1956 to 1969 and two derivatives of the Mead model (extended *RIC*, eRIC, and augmented *RIC*, aRIC) which were fully developed and thoroughly analyzed at UTEP in the past decade, served as the predicate circuit models of reference for the design of a novel, electrical ULF IOS respiratory impedance model which provides parameter estimates that physiologically parallel characteristics of subjects with SAD.

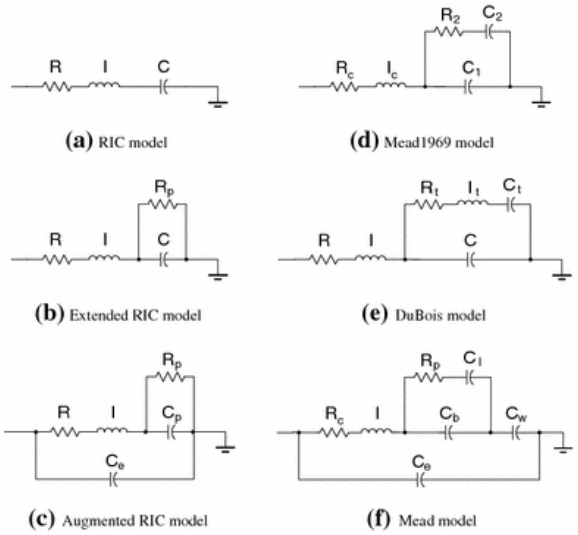

Figure 2.3: (a)-(f) Electrical analogs and reference models of the human respiratory system.

Using respiratory impedance analogs, translation of acoustic impedance to electrical impedance is accomplished by relating, first, the voltage drop across an electrical element to acoustic pressure drop relative to atmospheric pressure and, second, the electrical current through an element to volume velocity or airflow. Therefore, the acoustical impedance is made equivalent to electrical impedance, via analog component models, and its definition as the ratio of the pressure drop to the change in airflow in (2-2) is modeled as the ratio of voltage to current at various levels of the respiratory system model. In the electrical analog for the respiratory system, resistors represent central or peripheral resistance to airflow, and capacitors and inductors represent compliance and mass-inertive forces of the moving air column in conducting airways for high and low frequency of response, respectively, as detailed in Table 3.1.

All reference electric circuit models including ancillary component representations for peripheral resistance of the small airways, e.g. R_p, were of primary importance and a particular focus of interest for benchmarking purposes as in Otis and Mead-1969 models in Fig. 2.4 and two-compartment model in Fig. 2.5. Fittingly, in addition to the Otis model [26], there are a few other pertinent electrical models that meet this criterion. For example, the Mead-1969 model [22], Mount model [34, 35], and two-compartment model [27] all share relatively similar circuit configurations depicting compartmentalization of the large airways from the small airways, representing the latter via parallel pathway arrangement of elements. These "p" components represented as electrical elements in the peripheral zone of the circuit model enable analysis of the SAD analog by demonstrating an inverse relationship between Z_{rs} and frequency, especially in the ULF range. Thus, a main objective of this research is to analyze changes in the mechanical properties of the lungs through corresponding changes in acoustical impedance when subjected to ULF IOS via a SAD model of the human respiratory system.

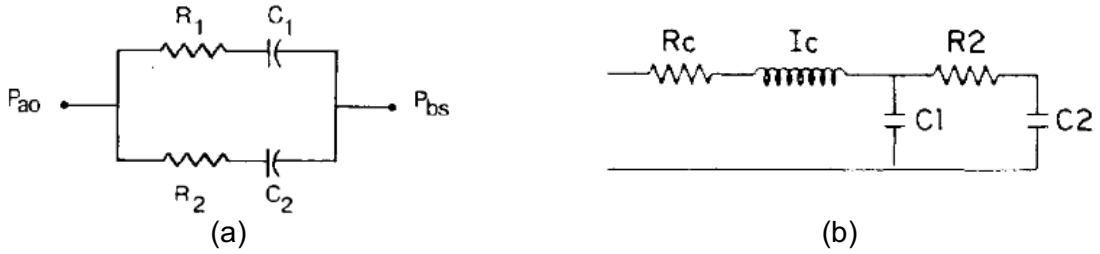

Figure 2.4: Electric analog of (a) Otis and (b) Mead-1969 models. Frequency dependence of respiratory impedance at outputs are depicted as parallel pathways, each with a different resistance-compliance time constant.

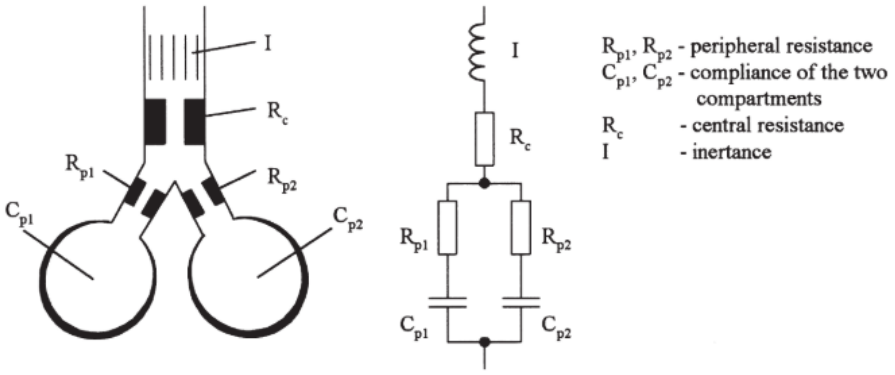

Figure 2.5: Electric analog of the parallel two-compartment model with accompanying lung model.

2.3.2 LOW FREQUENCY FOT

Conventional IOS testing covers an oscillation frequency range of test signal impulses from 5 to 30 Hz [13], with results as plotted in Fig. 2.1. Injection of high frequency (>20 Hz) pulses into the lungs mainly reach central airways, whereas low frequency (<15 Hz) pulses are transmitted distally into small airways. The difference between the resistances at these two distinct frequencies of pulses (i.e. R_5 minus R_{20}) is referred to as the frequency dependence of resistance (fdR) and is indicative of SAD, also referred to as SAI, when a large differential occurs. Additionally, at low frequencies, respiratory system behavior is dominated by the elastic recoil properties of the lungs, modeled as electrical capacitance; whereas, at higher frequencies the determination of impedance response is dominated by pulmonary inertance, modeled with electrical inductance, mostly attributable to diminished compliance of peripheral lung tissues and gas in airways.

Normally in the IOS test technique, five acoustic impulses per second, each approximately between 30 to 40 ms in duration, are applied at the airway opening alongside the patient's natural breathing via an inline mouthpiece coupled with an antibacterial filter [12]. This mixed multi-frequency approach avails IOS a higher SNR than mono-frequency FOT. Furthermore, the lower the frequency of the applied test signal, the deeper the oscillations travel into the lung periphery where the added compliance of multigenerational bronchioles and eventually the alveoli may influence the impedance calculation, i.e. as increased reactance, X_{rs}, with regard to the respiratory system frequency response. However, signal frequencies below 5 Hz are affected by harmonics of the underlying natural respiratory frequency, in the 0.3 to 0.5 Hz range in preschoolers, which contribute unwanted measurement noise [20]. Aside from the intensified vibrating sensation actuated in the subject's chest from this extended range into lower frequencies, which may be slightly more unpleasant to some while imperceptible to others, although otherwise safe, it is the interference from spontaneous tidal breathing that commonly discourages most researchers and equipment manufacturers from utilizing oscillations below 5 Hz as input pressure signals. Oftentimes, inferences by extrapolation of R_{rs} and X_{rs} curves in the ULF region are alternatively executed, but usually without merit and often disregarded in research and clinical practice.

A main aim of this research is the performance of an in-depth study of IOS ULF measurements and modeling designed to eliminate undesirable breathing frequency effects to reveal Z_{rs} values associated with small airway pathologies. The significance of this objective is the enhancement in measurement sensitivity of IOS for improved localization of site and degree of peripheral obstructions. In turn, this higher resolution examination of Z_{rs} below 5 Hz may lead to timelier, more accurate detection and treatment of distal obstructive diseases such as SAD and asthma.

CHAPTER 3: METHODOLOGY

A detailed description of methods, processes, and procedures utilized to address the presented objectives and the overall goal of this research are presented below.

3.1 IOS CLINICAL STUDY PATIENT DATABASE

An essential component that enabled the achievement of the objectives of this research was the use of a representative high-quality database that included the analysis of previously collected IOS data, centered on the classification of lung function with correlation between several demographic and anthropometric factors. This IOS lung function database was acquired in 2006 via the "Asthma on the Border" study conducted by UTEP researchers and funded by the NIH [12]. The database is comprised of 112 quality-assured records of male and female Hispanic and Caucasian minors, exclusively children between the ages of 5 to 17 years old, with each record consisting of respiratory impedance indices at discrete frequencies of 5, 10, 15, 20, 25, and 35 Hz. Furthermore, the raw IOS data and accompanying statistics were used to calculate the estimated IOS parameters of fdR, F_{res}, reactance area between X_5 and F_{res}, referred to as AX or the Goldman's Triangle, and eRIC and aRIC circuit model parameters that are also contained in the database. Results from this study were classified by the resident clinician, Dr. Michael Goldman, into one of four conditions of health or disease as Normal (N), Possible/Pre- Small Airway Impairment (PSAI), Small Airway Impairment (SAI), or Asthmatic (A) for each child record. Consequently, each record in the database belongs to a subset as either N, PSAI, SAI, or A. The sample size (n) for each subset of the four conditions of lung function varied with n = 11, 17, 54, and 30, respectively. Fig. 3.1 shows impedance measurement values with separate R_{rs} and X_{rs} plots with stratification of the IOS database population into the four classifications, indicating the

indistinct upper and lower boundaries for each and a real potential for crossover between adjacent groups; thus, demonstrating the need for a final clinical diagnosis by a qualified clinician.

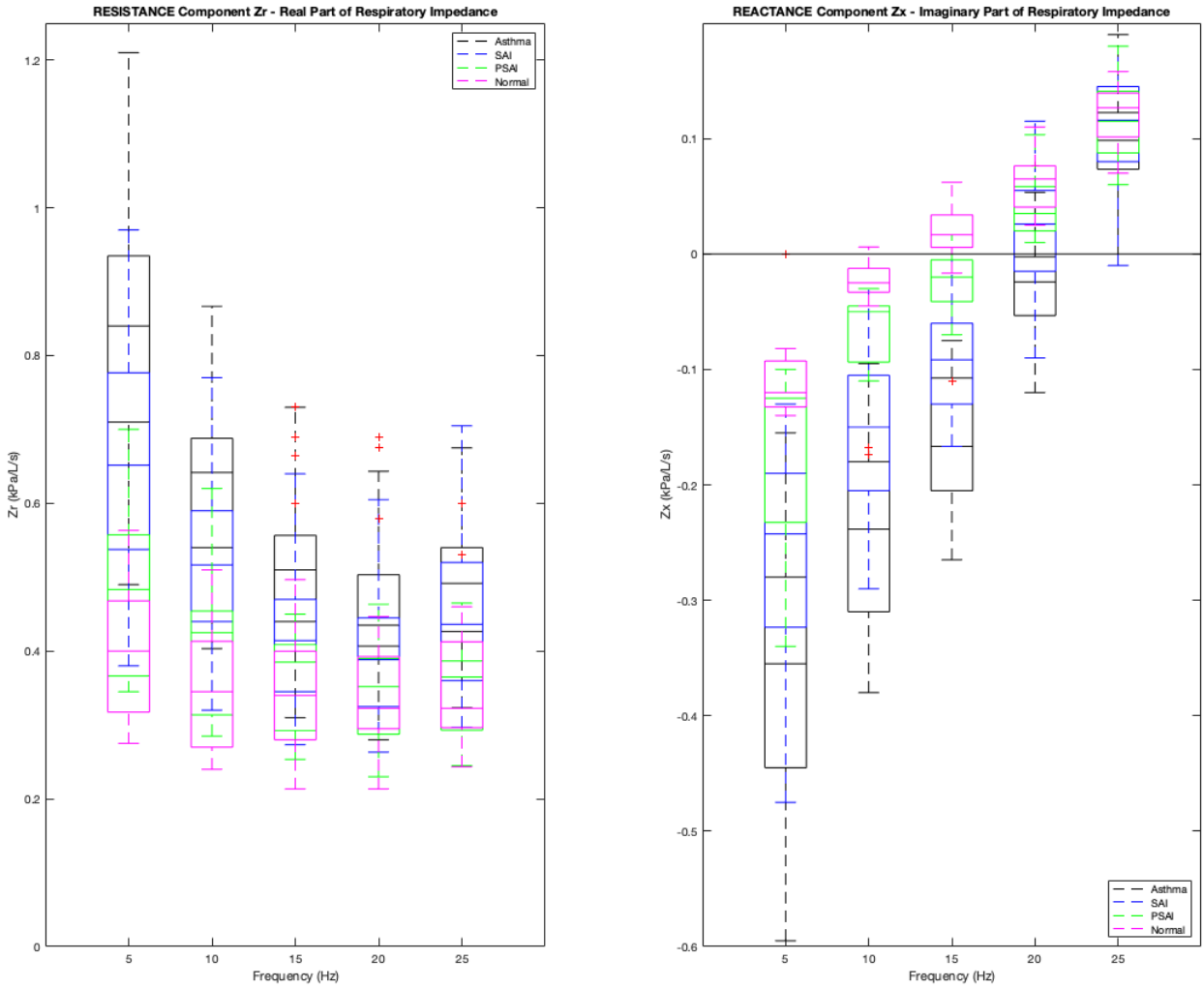

Figure 3.1: Comparison of 112 patient records from IOS database classified into four groups (asthma, SAI, PSAI, and normal) depicting ranges and variability in Zr and Zx measurements.

3.2 SAD Model – Research Design and Procedures

The earliest recorded attempt for modeling sinusoidal forced oscillation to acquire respiratory system impedance via an analogous mechano-acoustical representation of the chest and an equivalent electrical circuit was described in 1956 by DuBois *et al*. [14]. Several researchers

later proposed other linear and nonlinear lumped parameter models to represent the impedance of the total respiratory system through various architectures with resistive, inertive, and elastic components. Rather than relating to these components in mathematical or mechano-acoustical terms, several lumped parameter models aim to equate impedance parameters indirectly with the use of analogous components used in electrical circuits, namely resistance (R), inductance (I), and capacitance (C). Table 3.1 includes impedance measures in terms of the analogous relationships between quantitative physiological attributes of lung function, mechano-acoustical systems, and electrical circuit models.

Table 3.1: Analogous relationships of mechano-acoustical and electrical impedance to the mechanics of breathing.

PHYSIOLOGICAL		MECHANO-ACOUSTICAL	ELECTRICAL
TERM	UNITS		
Rate of Lung Volume Exchange (*inhalation/exhalation*)	L / sec	Air Flow	Current
Alveolar Air Pressure (*w.r.t. atmospheric pressure*)	kPa	Air Pressure	Voltage
Airway and Tissue Resistance	kPa / (L/sec)	Resistance	Resistance
Alveolar Air Capacitance	L / kPa	Capacitance	Capacitance
Tissue Compliance (*inverse of Elastance*)	L / kPa	Compliance	Capacitance
Tissue Inertance	kPa / (L/sec^2)	Inertance	Inductance

Furthermore, available models involve the use of mono-frequency FOT data to estimate impedance; while only a handful pertain exclusively to multi-frequency IOS and even fewer to ULF. Consequently, the present research focuses on the development and evaluation of a novel electrical analog to simulate the respiratory impedance response at ULF that pertains to lung function for patients with small airway disease, henceforth referred to as the SAD_{ulf} model.

Development of the novel SAD_{ulf} model began with a search for key theoretical electric circuit models that exhibited characteristics and exploited the unique discriminative property

inherent to IOS for simultaneous assessment of the contribution of central and peripheral airways to total respiratory impedance. The basic predicate models are shown in Fig. 2.3. As an illustration of modeling approach, the RIC model, oftentimes associated with a rigid tube and attached balloon mechanical analogy, offers a linear whole system model of a single-compartment structure. However, the RIC model does not discern between large and small airways impedance, as only total respiratory impedance is modeled. Further, fdR and frequency dependence of elastance of the lung are not replicated by this single-compartment model. Conversely, most nonlinear two-compartment models such as the eRIC model distinguish impedance of central airways from peripheral airways as parameters denoted with a subscript "*c*" for central or "*p*" for peripheral.

Aside from the number of compartments and irrespective of the quantity of elements, inclusion and arrangement of R, I, and C elements within electrical analogs is crucial in determining the frequency response from the respiratory system model to accurately ascertain physiologically and pathologically relevant impedance estimates. Compartmental arrangements of circuit elements may be in series or parallel to model effects such as fdR. One electrical analog in particular, the Otis model, as shown in Fig. 2.4, consists of a combination of both types; two parallel pathways each containing single R and C elements connected in series, representing the peripheral airways. Otis configured the circuit in this way primarily with the intention of expressing inhomogeneity in the lungs with varying degrees of obstruction from one region to another as evidenced by different impedance levels, resulting in unbalanced RC time constants (τ) between each pulmonary pathway [26]. Whereas, parallel ventilation heterogeneity in the lung must exist, even if purely on an anatomical basis, the concept of uneven time constants of the system implies that the left and the right system halves respond to airflow and pressure differently based on the regional severity of obstructions in the peripheral airways and/or restrictions on lung

elasticity [27]. When airflow stops, an air redistribution phenomenon occurs between both lungs via gas diffusion from the higher-pressure compartment to the lower-pressure compartment, in which ventilation of each separate lung may be quantified by mismatched time constants ($\tau_1 \neq \tau_2$) before equilibration [28].

To reproduce the significant qualities of the aforementioned electrical analogs as they relate to low frequency IOS testing, a two-compartment parallel pathways arrangement was chosen as the foundation for the design and development of the SAD_{ulf} model (Fig. 3.2). In this approach, and in accordance with Table 3.1, the SAD_{ulf} electrical model indirectly converts pressure to voltage and flow to current by means of replacing the mechano-acoustical model flow-resistive elements with electrical resistors and elastic compartments with capacitors. Since the focus of this research is the frequency response of the respiratory system to ULF test signal inputs, representation of inertance was omitted by design because inductor elements are insignificant at low frequencies given the model circuit when characterizing the peripheral airways. Therefore, the SAD_{ulf} model is unsuitable for dynamic analyses at frequencies higher than 25 Hz because the inertance of air and tissue are not included in the circuit model. Furthermore, while some electrical analogs, e.g. the aRIC model, choose to include an additional capacitor to model the extrathoracic compliance (*Ce*) in order to mitigate the effects of upper airway shunt, e.g. absorption of energy from acoustic impulse at high frequency due to friction and turbulence in the mouth and trachea, the SAD_{ulf} model excludes modeling of this extra element since its relevance pertains to impedance modeling at high frequencies. Finally, in regards to the first compartment, which models the contribution of the large central airways to the IOS impedance estimate, both airway resistance (*Rc*) and compliance (*Cc*) were contemplated as being significant in this region and therefore included at the front end of the SAD_{ulf} model.

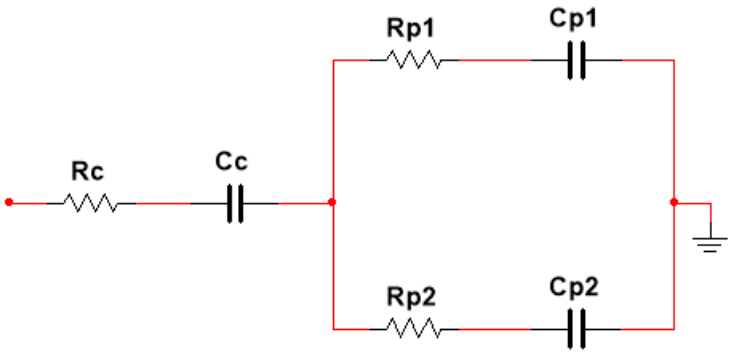

Figure 3.2: Schematic of electrical IOS model of SAD_{ul} for analysis at ULF. Rc and Cc represent the central airways resistance and compliance, respectively. Rp1 and Rp2 represent their respective pathway's resistive components of the peripheral airways' impedance; while, Cp1 and Cp2 represent their respective pathway's reactive components.

3.3 Inverse Modeling Approach: Parameter Estimation Technique

As reliable as IOS test measurements and indices such as AX and fdR are to the diagnosis of diminished lung function, particularly with respect to their discriminative abilities in revealing small airways impairment, it has been found that model-derived parameters may be just as, if not more, valuable and sensitive in their own regard for lung function monitoring and disease detection [37]. While standard IOS impedance measurements, plot tracings, and indices may offer very important information regarding metrics of pulmonary function, their interpretation is nontrivial due a lack of clear mapping between the test subject anatomy and pathology and the corresponding modeling and computations founded on electro-mechano-acoustical models. Use in this work of nonlinear regression for calculating model-derived parameters proved useful for describing physiological properties of the lung by attributing a tangible numerical value to specific lung regions, thereby simplifying clinical interpretations. Just as spirometry and IOS complement each other, together IOS indices and parameter estimates lead to more predictive and intuitive outcomes.

Establishing a mathematical model of a system whose configuration is not known a priori, in this case the structure of SAD_{ulf}, from experimental measurements of system inputs and outputs is referred to as inverse modeling. Black-box SAD_{ulf} parameters are evaluated by testing candidate internal mechanisms of the model's structure with varying inputs to see whether and how closely test results are matched given outputs provided by the experimental data set. Given that this is an ill-posed problem, a solution is sought through iterative steps to accurately estimate the predicted outputs within a minimal acceptable variance, i.e. estimation error within expected measurement error in the recorded experimental data. For this purpose, MATLAB® R2018b matrix-based programming language and software was utilized to calculate the parameters of the inverse model for the components of interest. In addition, Microsoft® Excel's add-in Solver program was similarly used, although primarily for visual and numerical validation, to perform what-if analysis on the same error minimization/solution optimization problem for model-derived parameter estimation by means of its GRG nonlinear solving method.

Having established the SAD_{ulf} respiratory system electrical analog, the next step was to determine whether or not impedance response at ULF could be properly inferred from the data set, which is shown in Table 3.2.

Table 3.2: Sample records from IOS pediatric patient database. Each subject record contains IOS respiratory impedance measurements recorded at five discrete frequencies: 5, 10, 15, 20, and 25 Hz; separated into both resistive and reactance information for a total of n=10 data points.

#	ID	Ethnicity	Sex	Age	Height (cm)	Weight (kg)	Classified by Dr. G as	R5	R10	R15	R20	R25	X5	X10	X15	X20	X25
1	7798	Caucasian	M	8	114.2	20.9	Asthma	0.94	0.68	0.51	0.41	0.46	-0.45	-0.33	-0.25	-0.08	0.11
2	111592	Caucasian	M	13	168.5	55.5	Asthma	0.57	0.49	0.42	0.37	0.41	-0.16	-0.10	-0.08	0.01	0.09
3	040496	Caucasian	M	10	139.7	40	Asthma	0.71	0.52	0.39	0.34	0.42	-0.28	-0.22	-0.15	-0.01	0.12
⋮																	
110	101600	Hispanic	M	6	127	25.1	SAD	0.63	0.53	0.44	0.37	0.40	-0.36	-0.18	-0.13	-0.02	0.10
111	123091	Hispanic	M	15	165.1	67	SAD	0.93	0.77	0.67	0.61	0.61	-0.25	-0.21	-0.15	-0.07	0.03
112	5491	Hispanic	F	15	165.1	77.9	Normal	0.36	0.29	0.30	0.30	0.29	-0.14	-0.02	0.04	0.08	0.13

Assigning valid parameters, or estimated values, to each element of the SAD_{ulf} electrical circuit via inverse modeling allows the calculation and prediction of respiratory impedance response below the standard IOS frequency range. This links and characterizes the influences of resistive and capacitive components on respiratory impairments that take part under specific physiological conditions, e.g. obstruction, specifically to small airways disease. For this inverse modeling approach, the units of measurement remain in terms of respiratory mechanics, where airways resistance (R) and tissue compliance (C) are left in the mechano-acoustical energy domain and denoted in terms kPa/L/s and L/kPa, respectively.

Equations that represent both the resistive Z_r and reactive Z_x components of the respiratory impedance Z_{rs} under low frequency IOS form the basis for inverse models of the lung. These models are used to derive the state of pulmonary function via frequency response computation, thus serving the main purpose behind the parameter estimation process. The impedance equation for the IOS SAD_{ulf} model, also referred to as the equation of motion is the following:

$$Z_{rs} = R_c + \frac{1}{j\omega C_c} + \left[R_{p1} + \frac{1}{j\omega C_{p1}}\right] \Big\| \left[R_{p2} + \frac{1}{j\omega C_{p2}}\right] \tag{3-1}$$

with the real and imaginary parts expressed as:

$$Z_r = R_c + \frac{\omega^2 \tau_{p1}\tau_{p2}(\tau_{p1}C_{p2} + \tau_{p2}C_{p1}) + \tau_{p1}C_{p1} + \tau_{p2}C_{p2}}{\omega^2 C_{p1}^2 C_{p2}^2 (R_{p1} + R_{p2})^2 + (C_{p1} + C_{p2})^2} \tag{3-2}$$

$$Z_x = \frac{1}{\omega C_c} - \frac{\omega^2 (\tau_{p2}C_{p1} + \tau_{p1}C_{p2})^2 + (C_{p1} + C_{p2})^2}{\omega^2 (\tau_{p1}^2 C_{p2} + \tau_{p2}^2 C_{p2}) + C_{p1} + C_{p2}} \tag{3-3}$$

where the angular frequency $\omega = 2\pi f$, and the time constants are $\tau_{p1} = R_{p1}C_{p1}$ and $\tau_{p2} = R_{p2}C_{p2}$, respectively. Thus, the equation of motion for the two-compartment SAD_{ulf} model is a second-order differential equation, which explicitly shows the frequency dependence of pulmonary system resistance and the reactive component of impedance, which is purely imaginary.

3.4 NONLINEAR LEAST SQUARES REGRESSION

For model parameter estimation, this work performs regression analyses through least squares minimization (LS) to produce best fit functions between dependent outcomes and independent predictors. LS is applied to estimate the parameters of the nonlinear electrical analog designed to compute the SAD_{ulf} impedance model. Parameter estimation, and extrapolation as discussed in chapter 4, was performed using MATLAB's built-in function *lsqnonlin*. Execution of *lsqnonlin* solves nonlinear LS curve fitting problems of the form:

$$\min_x \|f(x)\|_2^2 = \min_x (f_1(x)^2 + f_2(x)^2 + \ldots + f_n(x)^2) \qquad (3\text{-}4)$$

with optional upper and lower limits on the components of x. Hence, this translates into a curve fitting prediction routine, wherein the LS regression analysis minimizes the sum of squared residuals, $\epsilon_i, i = 1,2,..,n,$ where n is the data subset cardinality, between true impedance data at discrete frequencies as taken from the IOS patient database and the computed impedance solution.

For yielding the lowest estimation error, and therefore calculating optimal model parameter values, several factors were taken into consideration regarding the accuracy and robustness of the devised method to reliably converge to parameter values that are physiologically meaningful. The algorithm implemented in the MATLAB environment includes randomization of initial conditions, determination of the global minimum instead of local minima (as shown in an example in Fig. 3.3), definition of numerical constraints, establishing iteration step size and threshold for number of trials, and stopping criteria that avoids overfitting the model. The most impactful algorithmic steps are the random selection of initial estimate values and the designation of lower and upper bounds. The significance of the boundary constraints is to enable the algorithm's power for optimization of parameter values while avoiding physiologically unrealistic solutions. Therefore, in the SAD_{ulf} model, all R and C parameter estimates were constrained to real positive values $0 \ll$

$P_j \leq L_q, \forall j, q = r, c$ where L_r =1.5 kPa/L/s and L_c =1.5 L/kPa, respectively [29]. The result of plugging the optimized lumped parameter model estimates for all elements of the SAD_{ulf} circuit back into the Z_r and Z_x impedance equations is a best-fit function. Each component aptly approximated to predict respiratory system impedance response across the frequency range of interest in addition to the best combinations of parameter values for balanced/imbalanced τ_1 vs. τ_2 in specific cases, e.g., in dual- and parallel-compartment models such as Otis and SAD_{ulf}.

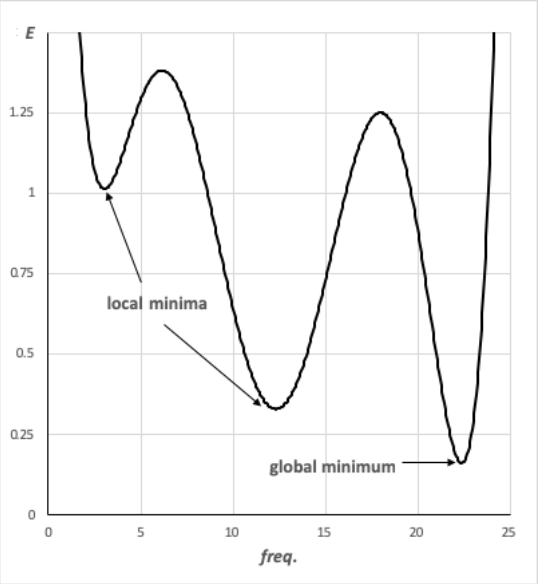

Figure 3.3: Global and local minima of an arbitrary error function, *E*. The presence of local minima stresses the importance of randomly selecting appropriate initial conditions for the least squares algorithm in order to determine the best approximation to the global minimum.

The algorithm for SAD_{ulf} model parameter estimation is presented in pseudocode next. Although the algorithm used in this research required substantial programming to solve the error minimization problem using the pediatric IOS data set, details of the working code are rendered as simplified readable descriptions of the MATLAB program development process.

1. Declare and initialize all scalar and vector variables:

a. Define and initialize a vector $\boldsymbol{p}$ to represent initial conditions of the model-derived parameter estimates for the LS algorithm, where the vector's length equals the number of parameters in the model.

b. Create a variable $\boldsymbol{p_r}$ and initialize it to a very large random number. The final numerical value of this variable is equal to the estimation error.

b. Impose numerical constraints to find a solution for the error minimization problem that makes physiological sense, albeit at the expense of potentially obtaining a high error. For instance, a lower bound of 0.0 yields nonnegative values while an upper bound L_q = 1.5 returns realistic parameter estimates with respect to lung airways resistance and lung tissue compliance.

c. Establish iteration step size and stopping criteria by incrementally changing parameter values from one iteration to the next via LS optimization.

i. Step size Δ may be defined as the following:

$$\Delta = \max[abs(\boldsymbol{x} - \boldsymbol{x}')] \ , \qquad (3\text{-}5)$$

where $\boldsymbol{x}$ is a vector containing estimated parameter values of the current iteration and $\boldsymbol{x'}$ represents the previous iteration estimates.

ii. A stopping condition is imposed by comparing these incremental changes to a real number very close to zero, ϵ_s = 0.5 E-05, and finally stopping when either the step size is smaller than ϵ_s or until a large number of consecutive runs (1,000) have been attempted.

2. For a user-defined number of trials of the estimation algorithm, execute the following during each trial and repeat the process until all trials are completed:

a. Initialize a uniformly distributed random number generator to a unique state, based on the current time as per system clock, which seeds the generator to produce a different sequence

of numbers after each time the algorithm is performed and avoiding repeating multiple times the same estimation when performing the nonlinear LS regression function.

b. Form an initial estimate. Using the uniformly distributed random number generator, populate initial $\boldsymbol{p}$. Each element of the vector corresponds with a model-derived parameter, or more specifically an electrical component provided in the respiratory system analog. To seed the random number generator with initial conditions that are physiologically feasible, initial guesses ranging from 0 to 5 for the values of the resistances and 0 to 0.5 for the values of capacitances are selected.

c. Execute the nonlinear LS regression function using the initial estimate and applying the predefined upper and lower parameter limits. Store the returned output arguments, estimated parameter values and the residual into vector $\boldsymbol{x'}$ and variable $\boldsymbol{r'}$, respectively.

d. While $\Delta > \epsilon_s$, repeat the following:

   i. Run the nonlinear LS regression function using the values stored in $\boldsymbol{x'}$ as the updated parameter. Store new estimates as vector $\boldsymbol{x}$, the smallest between residual these new estimated solutions and the impedance values from pediatric IOS dataset at 5, 10, 15, 20 and 25 Hz into variable $\boldsymbol{r}$.

   ii. Recalculate Δ with the latest values from $\boldsymbol{x}$ and $\boldsymbol{x'}$ using (3-5).

   iii. Assess the current iteration output arguments and take the following actions:

   If $\boldsymbol{r} < \boldsymbol{r'}$, then reset $\boldsymbol{x} = \boldsymbol{x'}$ and $\boldsymbol{r'} = \boldsymbol{r}$. Repeat from (d).

e. Check if algorithm found minima:

If $\boldsymbol{r'} < \boldsymbol{p_r}$, then set $\boldsymbol{p} = \boldsymbol{x'}$ and $\boldsymbol{p_r} = \boldsymbol{r'}$. Repeat from (d).

3. Return to the user a final set of model-derived parameter estimates, vector $\boldsymbol{p}$, which yielded the smallest estimation error, $\boldsymbol{p_r}$, either by stopping on $\Delta \leq \epsilon_s$or reaching the user-defined maximum number of iterations.

3.5 FORWARD MODELING APPROACH: ELECTRO-MECHANO-ACOUSTICAL TRANSDUCTION

Forward modeling of SAD_{ulf}, performed here through simulation, involves having a priori knowledge of the internal system architecture and attempting to computationally predict its output from a given input [28]. Following Dubois modeling of respiratory mechanics with an electrical analog system, simulation of lung function with respect to airways and tissue impedance allows exploration and analysis of the lung pathophysiologic mechanisms. Based on sound modeling practice, the SAD_{ulf} analog abstraction is not designed to perfectly represent a lung with the full complexity of a human organ. Instead, the purpose of the novel SAD_{ulf} design is to follow the mechanical behavior dynamics of both the central airways and the peripheral airways such that its application as a forward model follows the lung frequency-dependent pressure-flow relationships.

A goal of this research is the design and implementation of a forward modeling approach to simulate IOS response to ultra-low frequency via the SAD_{ulf} respiratory impedance model. However, modeling attempts to actually transduce the energy domains, along with their respective units of measure, from physical respiratory models of the lung to electrical constructs are scarce and incomplete in the literature. Hence, a key deliverable of this research is a novel transduction scheme for the explicit conversion of parameters from the mechano-acoustical energy domain to the electrical energy domain.

The equipment for acquisition of impedance measurements in the IOS pediatric data set used in this work is a Jaeger MasterScreen IOS; Vyaire Medical, Yorba Linda, CA, USA. Because

of this, the MasterScreen IOS pressure sensor/transducer was used as a reference for devising the method leading to the mechano-acoustical to electrical transduction presented here. The IOS pressure transducer measures differential pressure across a Lilly-type pneumotachometer (PNT) and is used to obtain pressure readings at the mouth with respect to atmospheric pressure.

For PNT differential pressure measurement, airflow is determined directly from the pressure drop over a small fixed resistance with a heated mesh screen, which is then converted to an analog voltage signal and scaled proportionately to the rate of flow. The piezoresistive transducer span, i.e., the output voltage from zero to full-scale pressure, is set in accordance with its supply voltage and the PNT range of linearity as per the manufacturer calibration curve. Thus, the transduction of energy domains used in the forward modeling approach of SAD_{ulf} circuit simulation was founded on this differential pressure to output voltage relationship. However, to calculate electrical impedance with Ohm's Law at least two of the variables must be known; whereas, in the case of the IOS pressure transducer, only output voltage can be determined. Hence, since the IOS patient database contains mainly impedance data and neglects to include any accompanying transducer outputs, mappable to voltage readings, such as measured pressure and airflow at the mouth, nor integrated volume, neither I nor R can be deduced from the final impedance results. Therefore, based on the principles of fluid dynamics, including the Venturi effect, Bernoulli's Principle, and Poiseuille's Law, as they pertain to respiratory mechanics, and through manipulation of impedance equations, a sensible transduction method was developed as documented in Table 3.3.

Table 3.3: Energy domain transduction scheme from mechano-acoustical to electrical values and units.

	MECHANO-ACOUSTICAL		ELECTRICAL	
Pressure	1 kPa	=	1 V	***Voltage***
Flow	1 L/s	=	1 mA	***Current***
Resistance	1 kPa / (L/s)	=	1 kΩ	***Impedance***

To transduce complex mechanical impedance into the electrical domain, both the imaginary reactive component and the real resistive component must be represented. Although Table 3.3 can be used to directly assign resistor values in the SAD_{ulf} forward model, it is necessary to add an extra step to the transduction system for assigning capacitor values. The formula for calculating capacitive reactance is:

$$X_c = 1/\omega C \ , \qquad (3\text{-}6)$$

where $\omega = 2\pi f$, f is the frequency in hertz, and C represents the capacitance in farads. Consequently, substituting the frequency of the forced pressure input, i.e. the impulse signal, injected into the SAD_{ulf} model for f and replacing Xc with the measured reactance value from the IOS patient database at that same frequency (e.g. Xc replaced by X_{20} in first serial compartment and X_5 in second parallel compartment), the equation can be rearranged to calculate the transduced value for the capacitance C from units of L/kPa to μF. However, one should consider that this capacitance value pertains to all capacitors per respective compartment of the circuit, which according to the SAD_{ulf} model's schematic in Fig. 3.2 refers to C_c for the central capacitance and both C_{p1} and C_{p2} for the peripheral capacitance. Since the two subscript "p" capacitors reside in different pathways representing the peripheral airways of the lungs, the total transduced value for capacitance must

be shared proportionally among both elements and can be determined from the equation for parallel capacitors:

$$C_{p1} \,||\, C_{p2} \; = C_{p1} + C_{p2} \;, \tag{3-7}$$

where $C_{p1} \,||\, C_{p2}$ is the total capacitance of the SAD_{ulf} circuit. The values for C_{p1} and C_{p2} are determined by proportionally distributing the total capacitance across both elements by taking the ratio of their respective IOS component values as previously computed in the inverse modeling parameter estimates optimization technique.

With a method of transduction as just described, real electrical values and units can be attributed to each of the electrical elements, input signal sources, and output frequency response in the SAD_{ulf} model for forward-modeling simulations in actual electrical terms; versus the standing practice of commonly labeling electrical element symbols in circuit schematics with counterintuitive mechano-acoustical terms. To the best of our knowledge, no similar method of transduction exists in the literature.

3.6 Electrical Model Simulations Using ULF Excitation Signals

National Instrument's Multisim circuit design software was employed in the schematic capture and simulation of a unique electrical circuit model that reflects the SAD_{ulf} respiratory system impedance response under test using ULF IOS. This circuit simulation software was utilized to elicit and analyze the frequency response of existing and novel (objective 1) electrical circuit models of the human respiratory system for the investigation of their performance and accuracy in demonstrating physiological equivalency to clinically recognized respiratory impairment conditions within the peripheral airways, namely SAD. In particular, output voltages and currents from simulations in forward modeling of these electrical analogs were measured,

manipulated, and interpreted to assess fdR from impedance calculations at frequencies below the standard 5 to 25 Hz range, and thus detect SAD through enhanced resolution of the small airways. ULF pressure analogs, 0.5 Hz or 5 Hz square waves, 300 mV_{pp}, 40 ms pulse width, superimposed onto a similarly low frequency sinusoidal signal, 0.25 Hz, 1.6 V_{pp}, which represents the spontaneous breathing of the test subject at 15 breaths/min, constitute the composite signal, or IOS excitation pressure input [13, 30].

Leveraging the results of the inverse modeling algorithm, every resistor and capacitor of the SAD_{ulf} circuit model was given a value corresponding with results of the nonlinear LS regression analysis, or more specifically a model-derived best-fit parameter estimate. Each element value was ascertained with this algorithm using *averaged* impedance data drawn from the mean R_x and X_x measurements of the separate subsets of N (n=11), PSAI (n=17), SAI (n=54), and A (n=30) classifications as recorded in the IOS patient database, where x = 5, 10, 15, 20, and 25 Hz. The component values obtained from this averaging procedure were then transduced from the mechano-acoustical energy domain to the electrical energy domain, with the respective elements labeled accordingly, as demonstrated in Fig. 3.4.

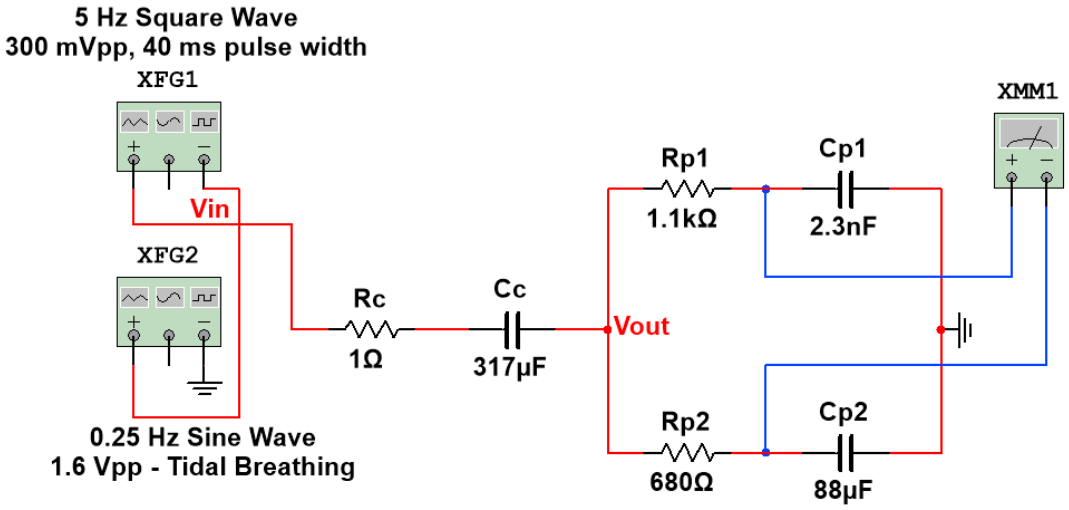

Figure 3.4: SAD_{ulf} circuit simulation representation of Asthma group for respiratory impedance determination at ultra-low frequency.

Next, using the software's Fourier analysis option, the SAD_{ulf} circuit simulation was executed to obtain the FFTs of both the output voltage *Vout* and current flowing through the parallel pathways I_{Cc}, at the fundamental frequency and for a specified number of harmonics appearing thereafter. The composite input signal fundamental frequency (f_0) was set at 0.5 Hz for obtaining ULF IOS response and at 5 Hz for acquiring the lower bound frequency response within the standard 5 to 25 Hz range, with the number of harmonics recorded being specified as eight and five, respectively. Furthermore, the simulation duration was set at 4 secs yielding up to 20 pulses with a 5 Hz square wave, with the transduced and digitized pressure and flow values, or *Vout* and I_{Cc} respectively, sampled at a rate of 200 Hz [31]. Finally, the values for Z_{rs} were calculated by dividing the FFTs of output voltage and current, as written in the following equation:

$$Z_{rs}(f) \mid_{m}^{n} = FFT[V_{out}] \Big/ FFT[I_{Cc}], \tag{3-8}$$

$$\text{where } m = \begin{Bmatrix} 0.5\ Hz, & for\ f_0 = 0.5\ Hz \\ 5\ Hz, & for\ f_0 = 5\ Hz \end{Bmatrix} \text{ and } n = \begin{Bmatrix} 4\ Hz, & for\ f_0 = 0.5\ Hz \\ 25\ Hz, & for\ f_0 = 5\ Hz \end{Bmatrix}$$

and $Z_{rs}(f)$ is evaluated across a narrow band spectrum at various incremental frequencies including 0.5, 1, 2, 3, 4, 5, 10, 15, 20, and 25 Hz. These forward model simulation results are then compared with their counterpart impedance calculations from the inverse modeling approach to determine model convergence.

CHAPTER 4: RESULTS – SAD_{ulf} RESPIRATORY MODEL ANALYSIS

A goal of the synthesis and use of ULF test signals in conjunction with recognized IOS circuit models would enhance the resolution of the respiratory system frequency response, particularly concerning the peripheral airways, to produce more informative IOS impedance results for an accurate and early detection of SAD and asthma. IOS impedance predictions and model-derived parameter estimates from computer simulations and modeling approaches successfully support this hypothesis as presented graphically, e.g. R_{rs} vs. ULF and X_{rs} vs. ULF plots, and statistically to analyze respiratory impedance data, validate the modeling techniques, and extract clinically and physiologically relevant information.

4.1 ENHANCED RESPIRATORY IMPEDANCE USING ULF IOS

Through this research, acoustical pressure oscillations, as represented by synthetic square wave impulses superimposed onto tidal breathing, were methodically applied and measured to characterize IOS test signal input oscillations, and thus allow determination of the respiratory impedance response Z_{rs} from the underlying tidal breathing component Z_{br} on the output signals in the frequency domain. However, the spontaneous breathing, which is considered by most researchers and clinicians as system noise, can be difficult to remove when dealing with ULF excitation signals. Due to overlap in the frequency range of interest for excitatory and output respiratory signals, filtering was not applicable for extracting the desired information from the blended IOS output signal, as done in practice with the 5Hz to 25Hz range.

Apart from conducting other filtering schemes and advanced signal processing practices, which are beyond the scope for this research, various other signal separation techniques, e.g. baseline approximation method as shown in Fig. 4.1, were contemplated regarding the IOS output

response to ULF to extract the Z_{br} from the Z_{rs} [13]. However, the combination of curve fitting, regression algorithms, and simulation sampling methods were ultimately sufficient for the accurate discernment and estimation of IOS ULF impedance without interference from the tidal breathing frequency content in the response signal.

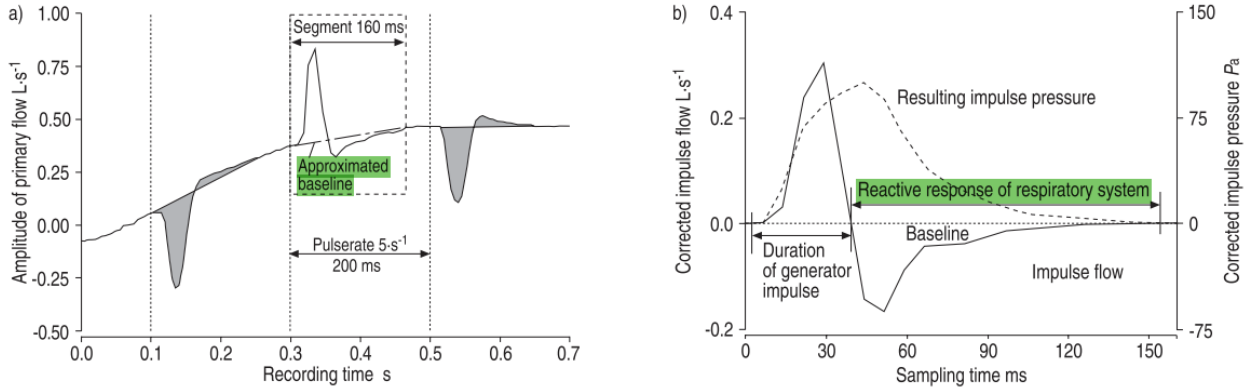

Figure 4.6: a) FOT primary flow exhalation response displaying loudspeaker-induced pulsatile flow superimposed onto the patient's expiratory respiratory flow. The dash-dot straight line segment is used to approximate respiratory flow only by disregarding the loudspeaker impulse. Subsequent application of this process to the recorded tracings of the composite flow (or pressure) signal, an undisturbed pure flow (or pressure) signal may be derived. b) Corrected impulse tracings of pressure (- - -) and flow (—) respiratory responses, resulting from baseline correction, now ready for input into the fast Fourier transform. Reprinted from *Lung Function Testing: Ch. 5-Forced Oscillation Technique and Impulse Oscillometry*, by H.J. Smith *et al*., Copyright 2005 by European Respiratory Society.

Consequently, corresponding R_{rs} and X_{rs} outputs could be unambiguously detected based on the selected test signals and resultant frequency response with notable trends and/or deviations across the lower spectrum of IOS frequencies attributed to the heightened sensitivity of the $\mathrm{SAD_{ulf}}$ model towards obtaining clearer recognition of respiratory state. Test signals were chosen based on their signal frequency, amplitude, morphology, and convenience in mathematical models and computer simulations.

4.1.1 INVERSE MODEL: OPTIMIZED PARAMETER SOLUTIONS

The objective of the followed inverse modeling approach is to define model-derived parameter estimates using algorithms in MATLAB and Excel to derive accurate and reliable predictions of respiratory impedance at ULF with IOS. These algorithms utilize impedance equations from (3-2) and (3-3), along with existing R_{rs} and X_{rs} measurements from the IOS patient database to perform nonlinear LS regression and minimize estimation error. Outcomes of these algorithms are presented in Table 4.1 with model-derived parameter estimates (R_c, C_c, R_{p1}, C_{p1}, R_{p2}, and C_{p2}) for each of the four respiratory conditions (N, PSAI, SAI, and A) and via plots of resistance (R_{rs}) and reactance (X_{rs}) components of the total input impedance of the respiratory system to provide visual verification of the SAD_{ulf} model.

Tables 4.1 and 4.2 display the obtained parameter estimates through the LS regression in the inverse model for Z_R and Z_X, respectively. Substitution of the corresponding values for these model-derived parameters into the equations of motion derives a predicted impedance value at any desired frequency, which provided a mathematical means for analyzing the SAD_{ulf} electrical analog for its practicality among the four classifications of respiratory impairment. Since the prime area of interest for this research are frequencies below 5 Hz, or the ULF range, for which no data exists in the IOS patient database, reference experimental data was unavailable and was not considered when constructing the algorithm for inverse modeling. Hence, in order to determine the resistance R_{rs} and reactance X_{rs} components of the predicted respiratory impedance response at ULF, the same optimized parameter estimates where used adjusting for the new lower frequency range, 0.5 to 4 Hz, in their respective equations.

Table 4.1: Resistance-based SAD_{ulf} model-derived parameter estimates from MATLAB LS-based algorithm and Excel Solver program for four classifications of IOS pediatric patient data. Units of measure for the parameter estimates of individual resistances and capacitances are kPa/L/s and L/kPa, respectively.

Z_R	NORMAL		PSAI		SAI		ASTHMA	
	MATLAB	Excel	MATLAB	Excel	MATLAB	Excel	MATLAB	Excel
R_c	0.3331	0.0010	0.2877	0.0010	0.1257	0.0010	0.2239	0.0010
R_{p1}	1.5000	0.4281	0.3838	0.5826	0.8084	0.6612	0.8725	1.1102
C_{p1}	1.5000	0.0662	1.2641	0.0253	0.7880	0.0191	1.3745	0.7277
R_{p2}	0.0010	1.5000	0.0706	0.8599	0.4019	0.9758	0.2557	0.6797
C_{p2}	0.0984	1.5000	0.0721	0.1410	0.0254	0.3739	0.0223	0.0141

Table 4.2: Reactance-based SAD_{ulf} model-derived parameter estimates from MATLAB LS-based algorithm and Excel Solver program for four classifications of IOS patient data. Units of measure for the parameter estimates of individual resistances and capacitances are kPa/L/s and L/kPa, respectively.

Z_X	NORMAL		PSAI		SAI		ASTHMA	
	MATLAB	Excel	MATLAB	Excel	MATLAB	Excel	MATLAB	Excel
C_c	0.0359	0.9303	0.0366	1.2292	0.0381	1.4820	0.0403	1.5000
R_{p1}	0.0010	1.5000	0.0010	1.5000	0.0010	1.5000	0.0010	1.5000
C_{p1}	0.0490	2.4E-5	0.0488	7.5E-6	0.0557	1.0E-9	0.0577	1.5E-5
R_{p2}	0.0162	0.0970	0.0152	0.0774	0.0141	0.0543	0.0130	0.0373
C_{p2}	1.5000	0.7487	1.5000	0.6233	1.5000	0.5287	1.5000	0.5833

The results of this modeling method for determining impedance within the standard IOS range, 5 to 25 Hz, were validated with Excel's Solver run in conjunction with the MATLAB implementation of the algorithm, also providing parameter estimates from the same dataset. Overall, both options performed equally well in minimizing the estimation error for resistance, as evidenced by resistance curves (via overlapping lines of R_{rs} measured and R_{rs} estimated) in Fig. 4.2 and the side-by-side comparisons in Table 4.3.

Table 4.3 also shows that in terms of minimizing the estimation error for reactance, the MATLAB algorithm provided better results. However, upon plotting the ULF predicted

impedance results, as shown in Fig. 4.2 and Fig. 4.3, it appears that the MATLAB algorithm potentially overfitted the model using a higher-order polynomial than the one in Excel. Best fit polynomial plots of reactance (Fig. 4.3) for both methods suddenly and sharply diverged at and below 5 Hz with the line representing Excel Solver's impedance solution following the expected trend, i.e. going downwards and having more negative values of reactance, while the line for the MATLAB algorithm actually began to ascend towards the x-axis from within the ULF range. This divergent behavior of the MATLAB reactance prediction was incited by an overfitting of parameter estimates to find the smallest estimation error possible, which also accounts for the discrepancy in parameter estimates values in Tables 4.1 and 4.2. Therefore, even though reactance obtained from the MATLAB algorithm appeared graphically valid within the standard 5 to 25 Hz range, not only matching the IOS measured data points but also the predicted Excel reactance data; those impedance predictions calculated by the MATLAB algorithm under 5 Hz are unreliable. Therefore, the Excel GRG nonlinear solver was the preferred method for determining optimal SAD_{ulf} model-derived parameter estimates only for reactance. Using MATLAB in this instance solely for the purpose of validating Excel's ULF reactance predictions by extrapolating the impedance curves of the measured IOS data, R_5 through R_{25} and X_5 through X_{25}, from the patient database, to plot, and attempt to mirror, Excel's predicted impedance at ULF; which, it did.

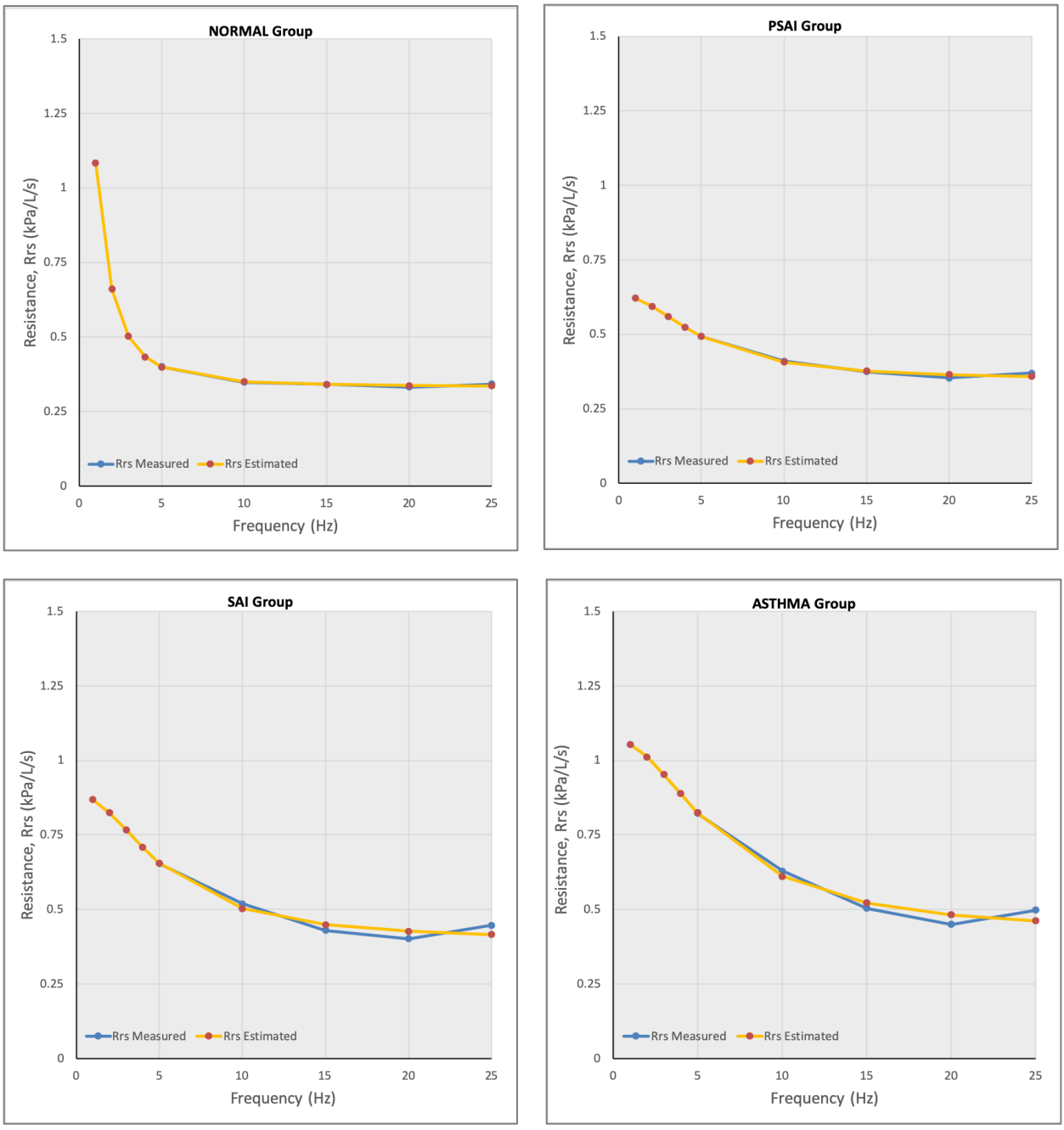

Figure 4.2: Resistance (Z_R) curves for IOS group average data and model estimates of Normal, PSAI, SAI, and Asthma classifications per Excel Solver.

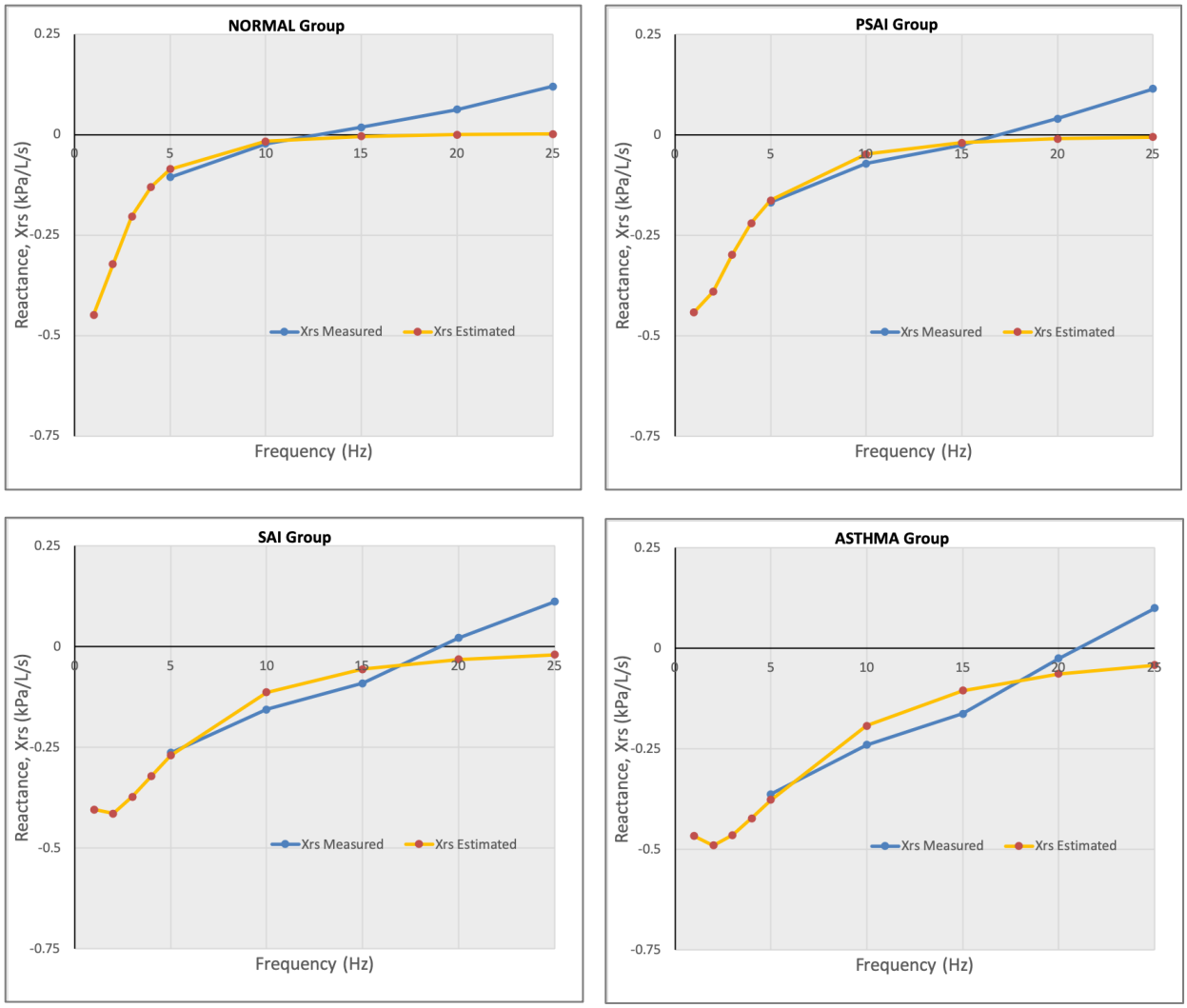

Figure 4.3: Reactance (Z_X) curves for IOS group average data and model estimates of Normal, PSAI, SAI, and Asthma classifications per Excel Solver.

Table 4.3: Estimation errors from SAD_{ULF} inverse model parameter estimation. A comparison between MATLAB and Excel nonlinear least squares algorithms per lung function classification for group average test results.

	Z_R LS error		Z_X LS error		Z LS error	
Classification	MATLAB	Excel	MATLAB	Excel	MATLAB	Excel
Normal	0.0001	0.0001	0.0027	0.0189	0.0028	0.0190
PSAI	0.0003	0.0002	0.0044	0.0174	0.0047	0.0176
SAI	0.0023	0.0023	0.0086	0.0232	0.0109	0.0255
Asthma	0.0030	0.0030	0.0133	0.0272	0.0163	0.0302

Finally, observing a similar divergence of plotted (reactance) curves in Fig. 4.3 on the opposite end of the spectrum, this is attributed to the SAD_{ulf} model's lack of inductors, which represent the inertance components of the proximal and distal airways. Since the inertance of the lungs dominates the composition of the reactive components of respiratory impedance for all frequencies greater than F_{res}, discrepant behavior of the SAD_{ulf} model at higher frequencies is to be expected, particularly because compensation for the effect of extrathoracic compliance (*Ce*) in the model was not included.

4.1.2 FORWARD MODEL: ACHIEVING INTUITIVE SIMULATIONS

In fulfillment of objective 3 of this dissertation, comprehensive simulations with the SAD_{ulf} model were conducted. With a working and valid transduction scheme in section 3.5, as described in Table 3.3, parameter estimates obtained through the inverse modeling approach became more intuitive from the network analysis perspective. Instead of having to deal with a mechanical to electrical model conversion in which electrical component values are expressed in mechanical units, the forward modeling approach described here is handled in fully electrical terms based on transduced units and on the transduction factors in Table 3.3. Leveraging this method for transformation from the mechano-acoustical to electrical energy domain, forward modeling of the SAD_{ulf} model resulted in the schematic capture and analysis of circuit parameters that explicitly express the foundational concepts and relationships behind IOS pressure and flow measurements/impedance predictions from inverse modeling results in realistic and measurable electrical terms and units.

Simulations of electronic circuits representing SAD_{ulf} forward models, such as the one depicted in Fig. 3.4, were executed in Multisim. Four versions of the SAD_{ulf} circuit were

constructed and analyzed, by mapping the values of resistors and capacitors in accordance with Tables 4.1 (R_c) and 4.2 (C_c, R_{p1}, C_{p1}, R_{p2}, and C_{p2}), with each version representing the four respiratory conditions as classified in the IOS patient database. Pertinent plots of the Multisim analysis for two IOS excitation signal scenarios under the four conditions, each with distinct parameter estimates, are presented in Fig.'s 4.4, 4.5, 4.6, and 4.7.

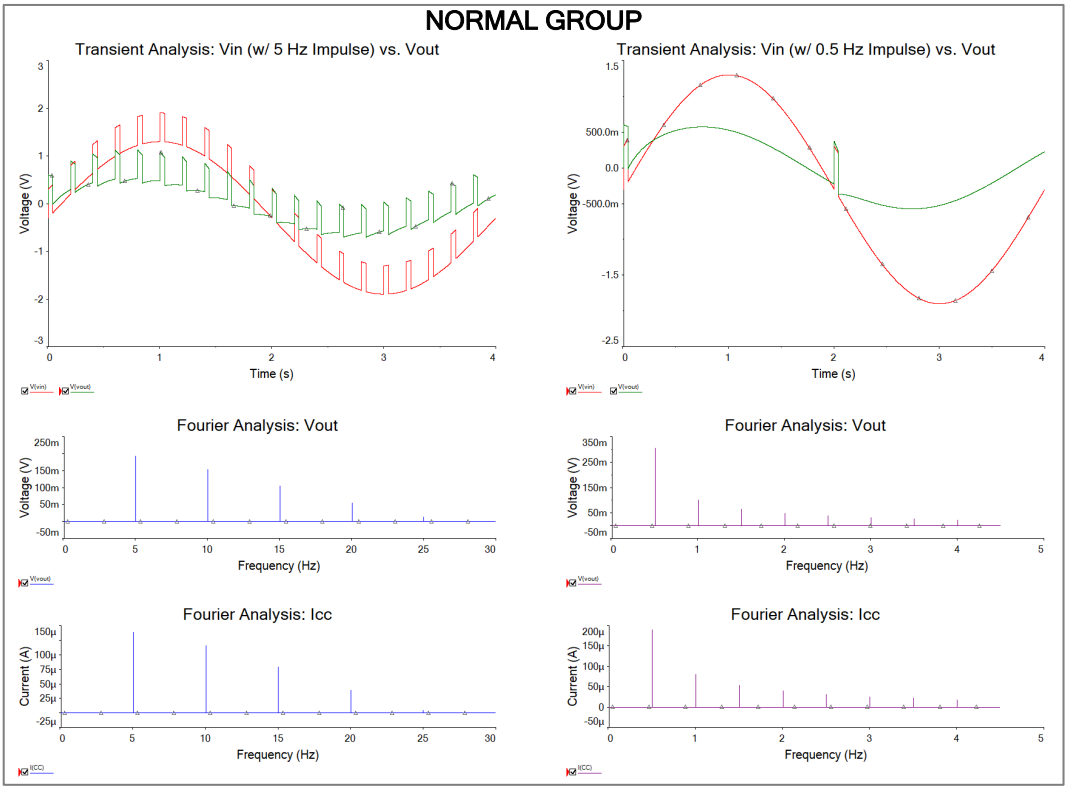

Figure 4.4: Simulated outputs from transient and Fourier analyses of the Normal SAD_{uif} model.

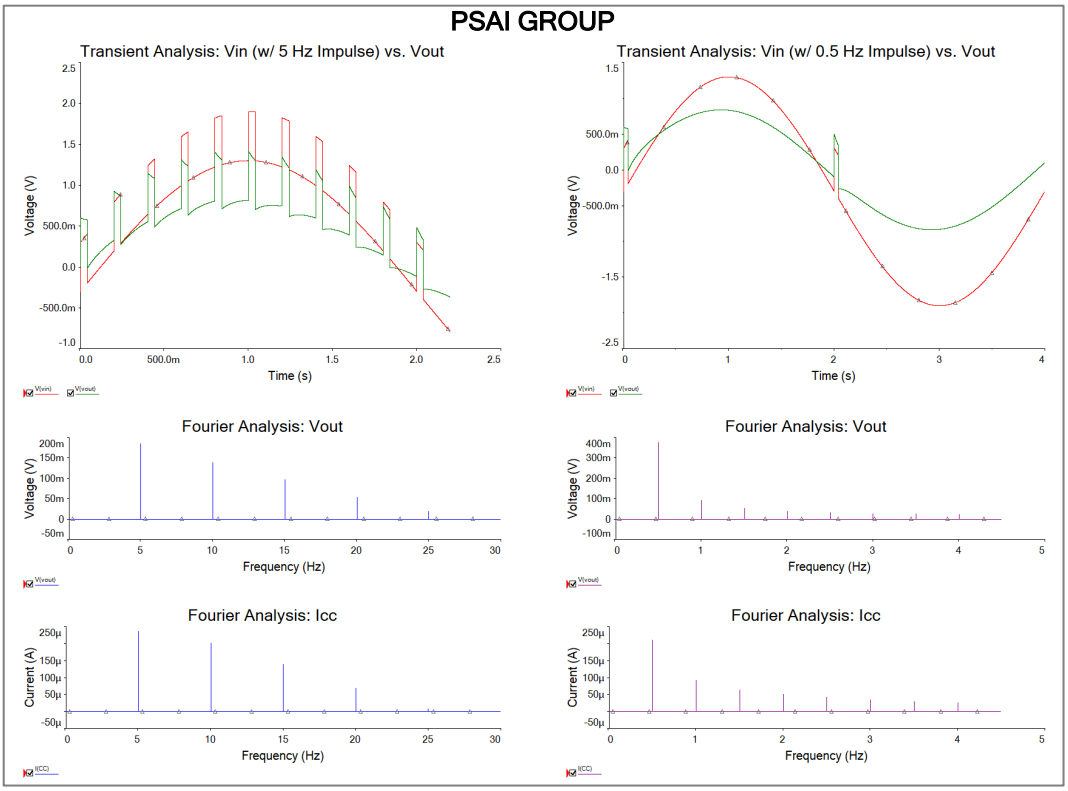

Figure 4.5: Simulated outputs from transient and Fourier analyses of the PSAI SAD_{ull} model.

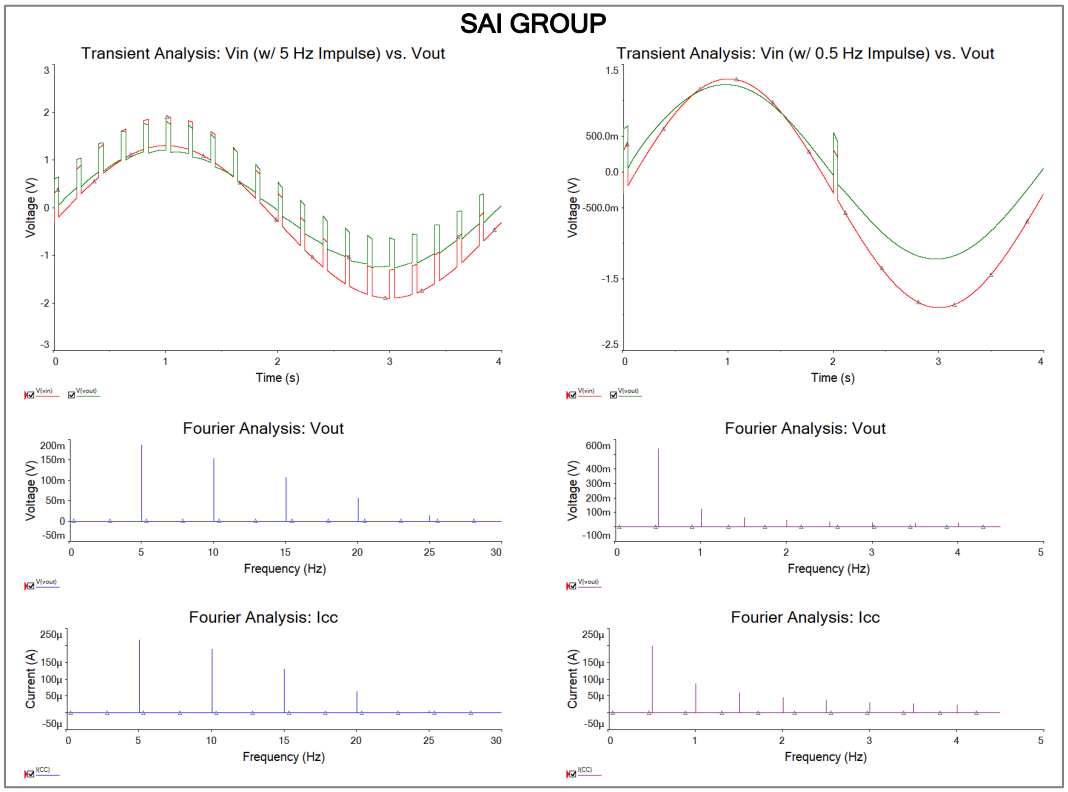

Figure 4.6: Simulated outputs from transient and Fourier analyses of the SAI SAD_{ull} model.

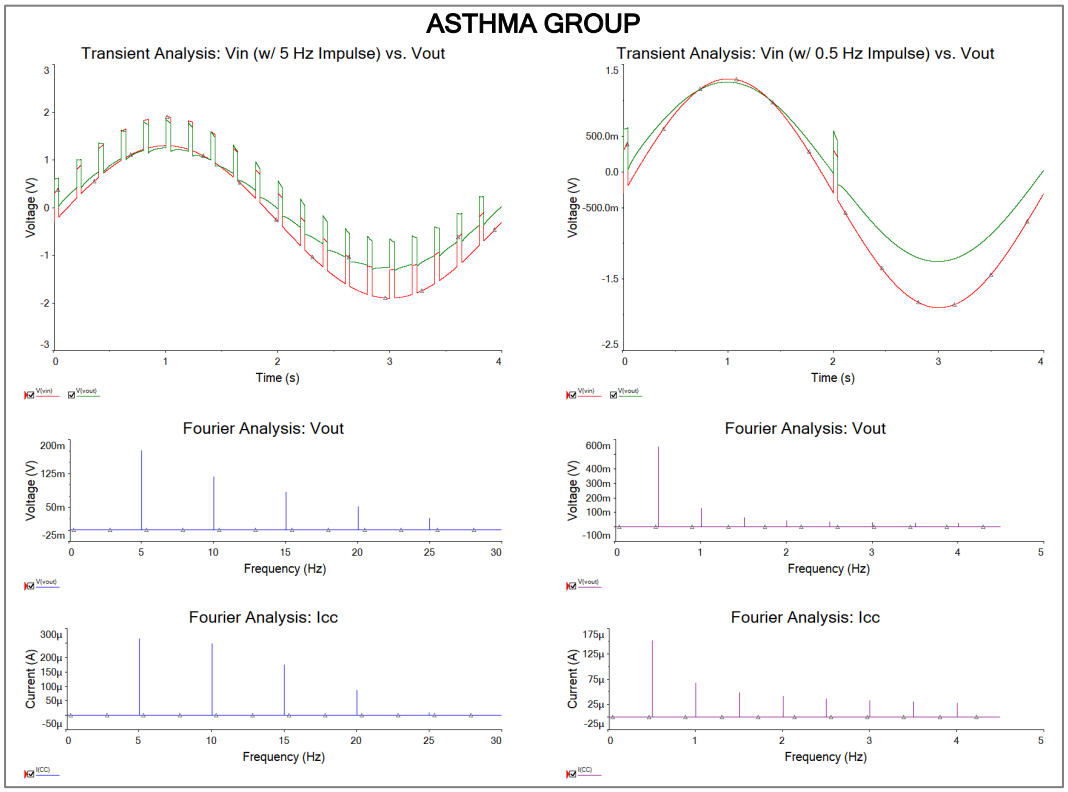

Figure 4.7: Simulated outputs from transient and Fourier analyses of the Asthma SAD_{ulf} model.

Circuit analysis consisted of AC analysis, specifically transient analysis and Fourier analysis for the four respiratory classification groups, performed for the two scenarios of composite test signals applied at the circuit's input (0.5 Hz or 5 Hz square wave sources; refer to section 3.6). Transient analysis was conducted to verify the validity of the superimposed signal from the voltage sources at *Vin* in the time domain with respect to waveform morphology, amplitude, phase, period, and pulse width of square wave; and also, to measure the resultant output signal frequency response at *Vout*. Fourier analysis provided the method for converting the SAD_{ulf} output signal from the time domain to the frequency domain. Characteristics of the frequency response at the output are the magnitudes of *Vout* and $I_{Cc'}$. Determining these values leads to the calculation of Z_{rs} with equation (3-8).

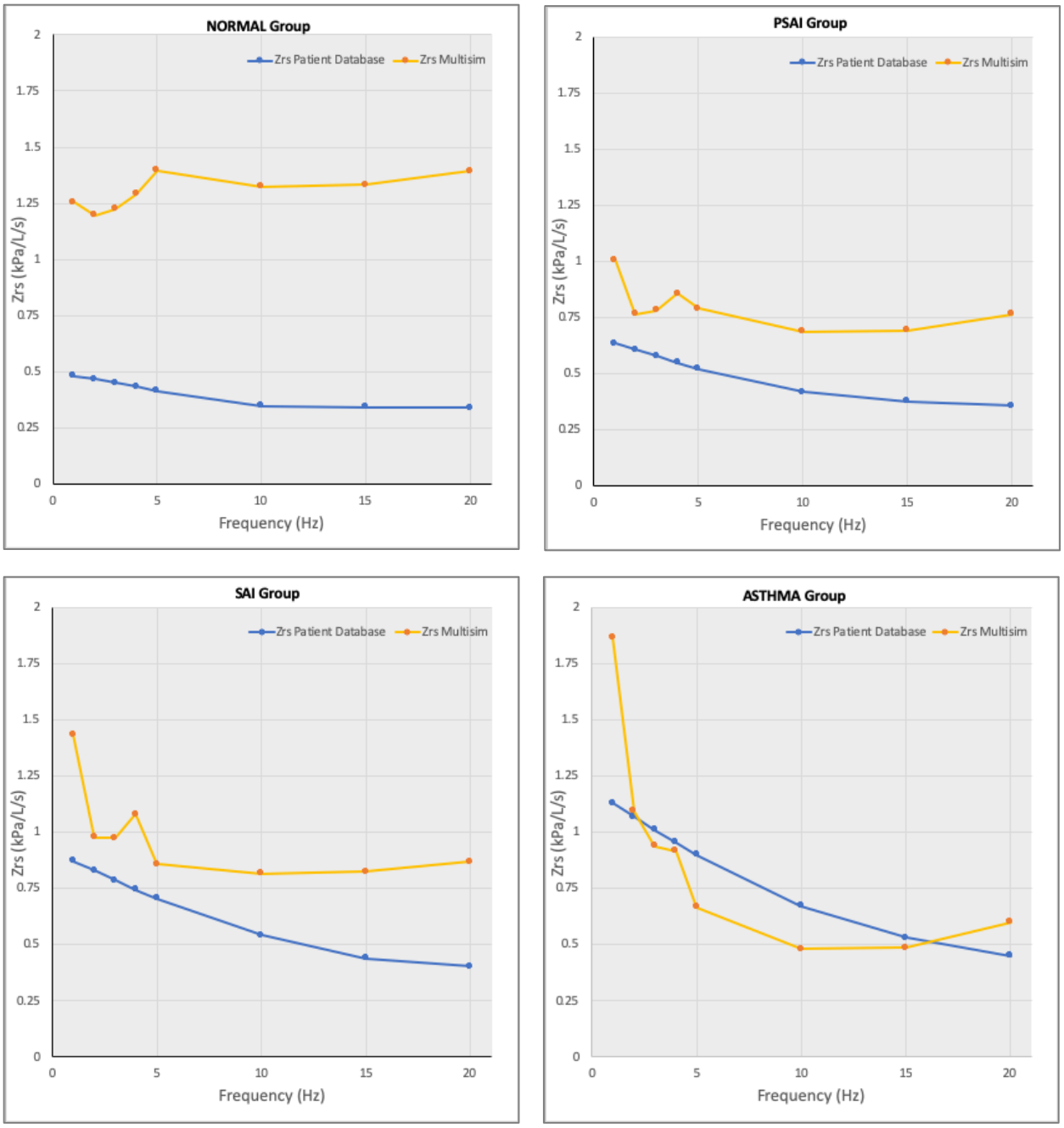

Figure 4.8: Z_{rs} plots of IOS group average data and model estimates for Normal, PSAI, SAI, and Asthma classifications per Multisim FFTs.

The ratio of the FFTs of *Vout* to I_{Cc} of the circuit analogous to Z_{rs} was then transduced from electrical impedance back to the mechano-acoustical domain in kPa/L/s, which was then plotted over the entire frequency range of 0.5 to 25 Hz for each of the IOS classifications (Fig.

4.8). Furthermore, for the purpose of comparing the forward modeling results to the measured impedance data from the IOS patient database, as done for inverse modeling, the R_{rs} and X_{rs} at discrete frequencies of 5 to 25 Hz were combined to formulate the total respiratory system impedance Z_{rs} per the equation:

$$Z_{rs} = \sqrt{R_{rs} + X_{rs}}\ . \qquad (4\text{-}1)$$

Results of this calculation derived from the IOS database impedance data, coupled with MATLAB extrapolated data points for the ULF range, were plotted against the forward model solutions. Fitted curves for the measured vs. predicted values for assessment of the validity and robustness of the forward modeling approach are shown in Fig. 4.8.

4.2 SAD_{ulf} Model Validation

In the case of objective 4, the performance evaluation of the SAD_{ulf} model was centered on defining its power and limitations in reliably determining SAI via IOS simulations within the ultra-low frequency range. Hence, the accuracy of IOS parameters estimation of the two-compartment parallel respiratory model was investigated, referring back to the eRIC and aRIC model parameter estimates and respective estimation errors made available in the IOS patient database for comparison. In conjunction, the IOS simulation results of the SAD_{ulf} model for the calculated respiratory impedance were also compared against the IOS patient database values across the Normal, PSAI, SAI, and Asthma classifications.

The coherence function and SNR were considered for validation of performance indices for the efficacy of the inverse and forward modeling approaches, sensitivity of electrical respiratory models at ULF, and adequacy of impedance parameter estimates. This was due to the fact that, in practice, evaluation of SNR for IOS input test signals and output responses to monitor

the effects of system noise on IOS circuit models and parameter estimates evaluate the performance of respiratory system frequency response under varying conditions throughout simulations. SNR was of interest, particularly within the ULF range due to competing Z_{br} and Z_{rs} measurements, to determine the validity of the response. As a second potential index, the coherence function, which reflects the linearity of the system and the quality of the output signal, may be calculated using the following equation:

$$\gamma^2(f) = \frac{|G_{pv}(f)|^2}{G_{pp}(f) \cdot G^*_{vv}(f)}, 0 \leq \gamma^2 \leq 1, \quad (4\text{-}1)$$

where G_{pv} is the cross-power spectrum between pressure and flow, and G_{pp}, G_{vv} are the auto-power spectrum of pressure and flow, respectively [23]. In PFT practice, the rule of thumb is to only accept impedance measurements with a $\gamma^2 \geq 0.9$ for most frequencies to ensure the measurement error is less than 10% [23]; although, a $\gamma^2 \geq 0.6$ may be an acceptable threshold at 5 Hz [13]. However, neither the SNR nor the coherence function can be calculated from results obtained from the SAD_{ulf}, though they could be considered as the basis of future model development work. Instead, Mean Absolute Error (MAE) was calculated to provide a measure of the goodness of fit among the modeling techniques.

For independent validation of model computations, Excel was utilized to perform all pertinent modeling calculations, perform extrapolations, generate plots, create tables, and prepare performance comparisons and sensitivity analyses amongst versions of the SAD_{ulf} circuit models using different impedance equations. The SAD_{ulf} circuit layout, configuration, and simulation technique were determined based on analysis of the effects of these factors on modeling small airway compliance and resistance in a robust manner.

4.2.1 PERFORMANCE EVALUATION

Performance evaluation determines the effectiveness of SAD_{ulf} inverse and forward modeling parameter estimation algorithms and circuit simulations to predict impedance that matches IOS patient data within measurement error. Therefore, accuracy of the measuring device, in this case the Jaeger MasterScreen IOS described in section 3.5, is compared to the percent error of the modeling approaches, i.e. error from Z_{rs} output of forward model and error from Z_{rs} output of inverse model. According to Vyaire Medical, the original equipment manufacturer, the accuracy of the MasterScreen IOS hardware, inclusive of the pneumotach and pressure transducer, is $\pm 2\%$, under the assumption that calibration is performed regularly.

Calculation of the error attributed to the SAD_{ulf} model inverse and forward modeling approaches were determined via MAE of estimation results, which remain dependent on the modeling algorithm as well as the IOS respiratory condition. MAE is calculated according to the following equation:

$$MAE = \frac{1}{n}\sum_{0.5}^{4} |r_i(\boldsymbol{p})| , \qquad (4\text{-}2)$$

where i = 0.5, 1, 2, 3, and 4 Hz, n = number of impedance values, and $\boldsymbol{p}$ = parameter estimate vector.

Due to lack of measured impedance for ULF in the IOS patient database, no direct comparison with predicted values could be made for the range of 0.5 to 4 Hz. Two approaches to address this situation were taken: 1) MAE was derived for the two inverse modeling parameter estimation algorithms in MATLAB and Excel. For the forward modeling impedance estimation technique with Multisim, impedance values calculated in the standard 5 to 25 Hz range are compared against one another and referenced with IOS measured data in Table 4.4. And 2) MAE

was recalculated using the predicted impedance values in the ULF range of 0.5 to 4 Hz from these models, with reference to extrapolated data in Table 4.5.

Table 4.4: Measured and estimated impedance for representative child patient with asthma, with MAE for inverse and forward models over the standard IOS frequency range.

	Z_5	Z_{10}	Z_{15}	Z_{20}	Z_{25}	*MAE*
Measured	0.899	0.673	0.530	0.450	0.508	
MATLAB	0.825	0.611	0.522	0.482	0.462	0.0444
Excel	0.826	0.612	0.523	0.483	0.463	0.0438
Multisim	0.667	0.480	0.485	0.601	3.130*	0.1553

* invalid data, not included in MAE; divergent impedance curve beyond 25 Hz due to high frequency inertance not included in the SAD_{ulf} model.

Table 4.5: Extrapolated and estimated impedance for representative child patient with asthma, with MAE for inverse and forward models over the ULF IOS frequency range.

	$Z_{0.5}$	Z_1	Z_2	Z_3	Z_4	*MAE*
Extrapolated	1.159	1.129	1.069	1.011	0.954	
MATLAB	1.065	1.054	1.012	0.953	0.888	0.070
Excel	1.066	1.054	1.013	0.954	0.890	0.069
Multisim	3.654*	1.869	1.094	0.938	0.915	0.219

* invalid data, not included in MAE; divergent impedance curve below 1 Hz due to low SNR.

From these results, it is observed that the inverse modeling parameter estimation performed fairly well with a low MAE. Data sets of impedance values derived from MATLAB and Excel were nearly identical irrespective of frequency range, thus validating the SAD_{ulf} model. However, it is important to note that the SAD_{ulf} model impedance equation is governed by a second-order equation, yet the MATLAB and Excel algorithms employed higher-order polynomial functions to fit the impedance data, which may potentially result in overfitting the model as observed at the lowest frequencies in Fig. 4.3. Whereas, in the case of circuit simulation results using Multisim FFT impedance data, the MAE was higher than expected. Therefore, as this method of assessment

for the SAD_{ulf} model seemed very appealing at first, especially since it enabled the introduced novel transduction of parameter estimates into the appropriate energy domain, it was decided that the proposed forward modeling approach cannot be used effectively at ULF as is, but perhaps it eventually may be further refined for this technique.

CHAPTER 5: DISCUSSION

Detection and diagnosis of small airway disease and asthma is oftentimes a difficult task, especially in young children where variability among their statures and still developing physiques often conflicts with acquiring reliable measures of their lung's respiratory impedance. In this case, and in accordance with the outcomes of the research objectives of this dissertation, a "one size fits all" reference equation as the typically accepted standard for classification is not recommended. Instead, since SAD has previously been identified as a likely childhood precursor for the pathogenesis of asthma, and it cannot be detected by spirometry, we suggest that researchers and clinicians take a deeper look into the lung's "quiet zone" through ULF IOS and its enhanced discriminative capacity for the early detection of the onset of this disease of the peripheral airways.

5.1 ULF Respiratory Impedance Response towards SAD and Asthma Detection

The relationship between SAD and asthma detection using IOS PFT within the typical frequency range of 5 to 30 Hz is well established across subject groups, as shown in Fig. 2.1. However, results lack reliability in the case of a single subject, particularly when attempting to quantify lung inhomogeneities via some functional representation of respiratory mechanics, e.g. catch-all IOS reference equations and models serving the general population, not intended to be anatomically specific [21]. For several decades, IOS researchers and clinicians have held to the 5 Hz lower threshold of pulmonary function testing primarily due to potential for concomitant low frequency spontaneous breathing signals to corrupt the low frequency respiratory impedance response, thereby compromising their IOS results in undetectable manner.

IOS impedance results in the frequency range below 10 Hz, however, are most sensitive to normal physical processes and pathologic structural alterations [11]. FOT studies that may relate

to ULF response are relatively scarce and date back to 1986 [22]. More recently, in 2017, Maes *et al*. [11] developed an FOT method using a fan-based apparatus to measure respiratory impedance within the normal tidal breathing frequency and applied it to a small group of healthy individuals. However, to the best of my knowledge, no work with ULF IOS is available in the literature.

As the basis of the research presented herein, particularly in reference to objectives 1, 2, and 3 in section 2, synthetic ULF IOS input test signals were generated in the 0.5 to 4 Hz range for the purpose of analyzing their effects on parameter estimation and sensitivity of respiratory impedance calculations via computer simulations of electrical circuit analogs of the human respiratory system. The upper and lower cutoff frequencies for this specific range were strategically selected to isolate Z_{rs} results from conventional IOS low frequencies, i.e. 5 to 15 Hz, while also considering the higher harmonics of underlying natural respiration frequency in preschoolers (0.33-0.5 Hz), respectively. Upon injection of these synthesized ULF excitation signals into a novel IOS SAD_{ulf} model focused on predicting the onset of asthma, it was expected that some type of amplified frequency response would occur, which would then hopefully lead to the discovery of SAD hallmarks from deep within the peripheral airways. This enhanced impedance response would better lend itself to an earlier and more sensitive detection of SAD.

5.2 Relationship of Model-Derived Parameters to IOS Indices

Examination of the relationships between relevant IOS indices that have historically been associated with assessment of the peripheral airways and ULF IOS estimated model-derived parameters were of particular interest to the findings of this research. An accurate and reliable determination of input respiratory system impedance at ULF IOS was supported in the previous chapter through inverse and forward modeling techniques, which were proven to be mostly in

accordance with trending results among the standard 5 to 25 Hz range both numerically and graphically, e.g. curve fitting of SAD model-derived parameters at ULF coinciding with back extrapolation of IOS measured impedance data. This finding is further substantiated by similar corresponding trends witnessed among two particularly SAD-sensitive IOS indices, namely fdR and AX, as is demonstrated below.

Table 5.1: IOS indices for frequency dependence of resistance (fdR=R_5-R_{20}) and reactance area (AX, or Goldman's Triangle) estimated over 5 Hz to resonant frequency (F_{res}) range and at ULF between 0.5-5 Hz.

fdR (kPa/L/s)	**Normal**	**PSAI**	**SAI**	**Asthma**	*AX* (kPa/L)
5-25 Hz	0.0678	0.1389	0.2528	0.3735	
ULF range	1.0444	0.1356	0.2248	0.2400	
	0.4151	*0.5237*	*2.7535*	*3.3664*	*5-25 Hz*
	1.1373	*1.4232*	*1.6401*	*2.0228*	*ULF range*

fdR is indicative of an imbalance in the levels of severity for obstruction or restriction amongst lower and upper airways. Negative fdR refers to a negative slope of Z_R from R_5 to R_{20}, and signifies greater impairment in the distal airways than in the proximal airways; precisely owing to IOS discriminative capacity for identification of regional inhomogeneity in the lungs. Reactance area (AX), on the other hand, is an IOS index intimately related to tissue compliance or elastance within the peripheral airways. AX may be defined as magnitude of Z_X in kPa/L of the low frequency impedance response integrated over the frequency range from 5 Hz to F_{res}. Evidence points to the fact that inflammation and constriction of the peripheral airways is a commonality among asthma patients, for which both of these IOS indices individually may contribute to the detection, diagnosis, and treatment of this small airways disease.

Examining fdR alongside AX, as shown in Table 5.1, may provide insights regarding combining the resistive and reactive components of respiratory impedance to obtain an indication of the source and location of what may be causing any respiratory distresses. Employing these indices in clinical IOS applications, such as tracking changes in lung dysfunction over the course of bronchodilation and bronchoconstriction exercises for the purpose of monitoring treatment regimens for asthma, is of special interest when disparities are recognized between varying degrees of a medication efficacy; particularly since fdR and AX reflect the degree of obstruction in the peripheral airways. Therefore, it is common practice to study them in tandem. In fact, in 2005, Goldman *et al*. suggested close similarities between fdR and AX, wherein the equally weighted influences of their respective magnitudes appear to offer a near complete assessment of peripheral airway mechanical function [32].

As evidenced by the results in Table 5.1 and Fig. 5.1, from fdR and AX analyses of the SAD_{ulf} model, it is apparent that a negative frequency dependence of resistance exists among all IOS respiratory conditions as well as a complementary frequency dependence of compliance. These relationships persist regardless of method of acquisition, specifically referring to the frequency range from which the fdR and AX measurements were obtained (0.5-5 Hz or 5 Hz to F_{res}). Furthermore, it is acknowledged that the fluctuating value of F_{res} plays a critical role in the determination of AX using the traditional method, i.e. effectively shifting the upper limit of integration; whereas, the calculation of AX at ULF imposes fixed boundaries. Hence, the resulting fdR and AX magnitudes and any incremental differences between IOS groups will typically be larger within the standard frequency range. However, all pertinent observations indicate that ULF fdR and ULF AX are both as significant as their traditional counterparts in describing the state of lung function; thus, imparting their worth toward enhanced SAD and asthma detection.

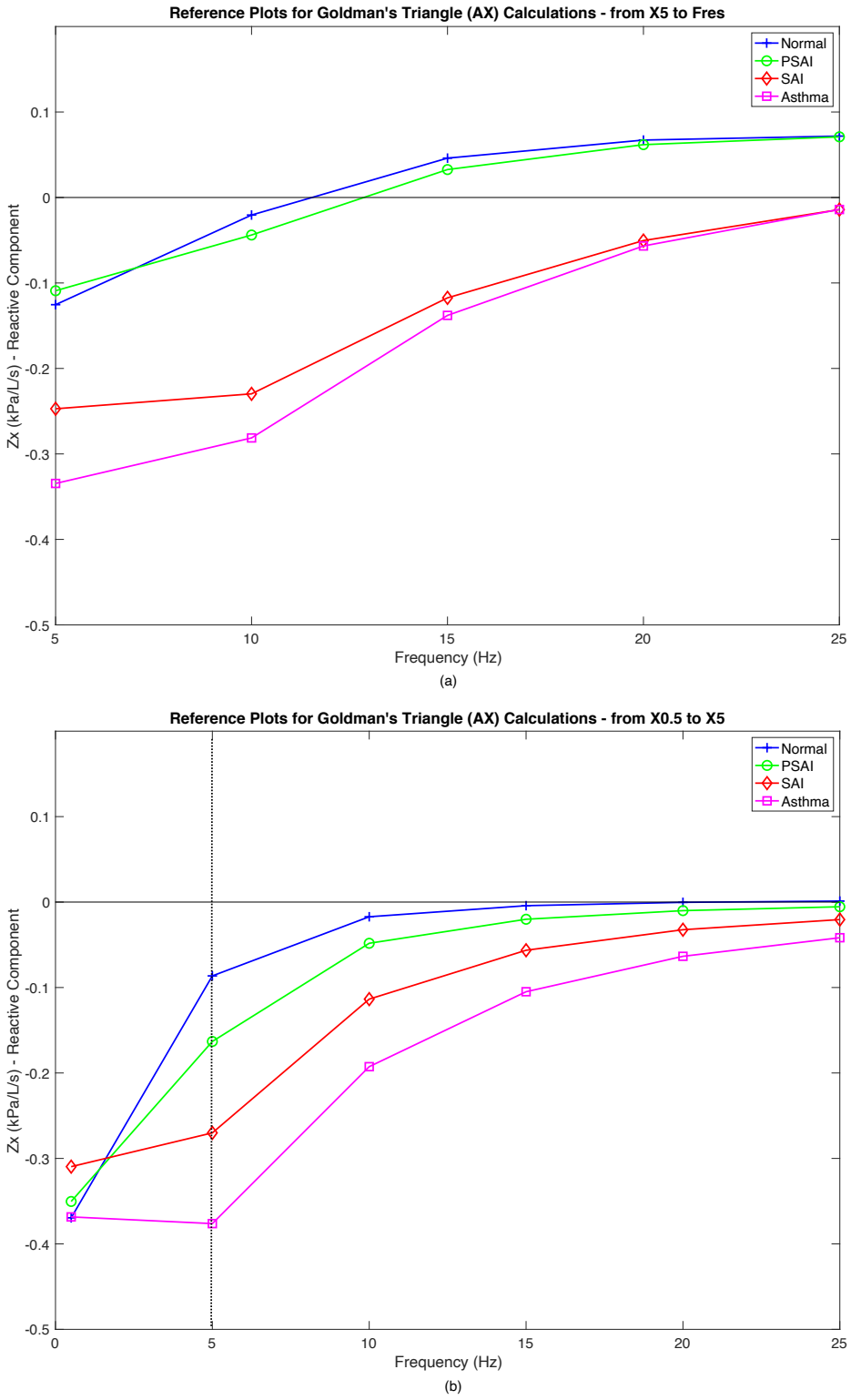

Figure 5.1: Z_X plots derived from SAD_{ur} model parameter estimates of group averages for Normal, PSAI, SAI, and Asthma classifications for AX determination. Post-processing of reactance data using MATLAB's integration function calculated the area above each curve up to the x-axis from (a) X_5 to resonant frequency and (b) $X_{0.5}$ to X_5 ULF.

5.3 SAD_{ulf} MODEL VERSUS PROMINENT EXISTING ELECTRICAL ANALOGS

Physiological interpretations based on SAD_{ulf} model fit to respiratory impedance data suggest that this model's elements and configuration are an accurate representation of the quiet zone's airway resistance and tissue compliance for determining the state of respiratory function in the small airways. The novel SAD_{ulf} model shares some features with the Otis, Mead-1969, and two-compartment models, as described in chapter 2, and may even be considered a hybrid of all three. The main difference being that the SAD_{ulf} model lacks any inductor elements due to the fact the new model focus is on the ULF range, thereby making any inductor in the circuit effectively a short-circuit at these low frequencies and therefore insignificant.

The SAD_{ulf} model's concept for parallel pathways was adopted to describe inhomogeneous lung ventilation between the peripheral airways of the right and left lungs and may even be interpreted further as modeling alveoli sacs in each respective lung should pressure and flow data be made available at this level. A unique characteristic of the SAD_{ulf} model is its ability to quantify the degree of inhomogeneity, which Glapiński *et al*. describe with a simple index defined as the ratio between longer and shorter time constants using the Otis model [36]. By effectively creating a Wheatstone bridge as its second compartment, i.e. peripheral parallel pathways of the circuit, the SAD_{ulf} model measures the differential voltage across the nodes located between the resistor and capacitor in each leg. This voltage is measured with a digital multimeter (DMM) across the model's bridge circuit as shown in Fig. 5.2. The balanced/unbalanced state of the parallel pathways' voltage dividers indicates the degree of inhomogeneity between the left and right lungs, with the sign of the resultant measurement indicative of which lung has higher impedance and thus poorer ventilation. Ideally, both lungs should be equally balanced and result in a zero voltage on

the DMM; however, in all practicality, the DMM reading will never be absolute zero because cardiogenic oscillations induce low amplitude noise into the left lung and cause a perpetual bias.

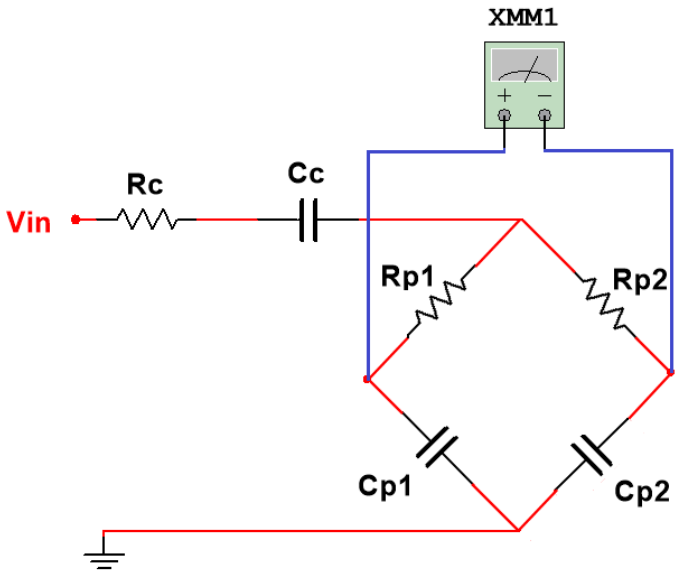

Figure 5.2: SAD_{air} model bridge circuit for measuring inhomogeneity between the lungs.

CHAPTER 6: CONCLUSIONS

Clinical adoption of IOS is still lagging behind spirometry due to the complexity involved in analyzing IOS results, which may be relatively intuitive for engineers/scientists familiar with electrical models and analogous references to pulmonary "impedance", but not particularly so for clinicians or physicians; especially those who struggle to visualize and relate these electro-mechano-acoustical concepts with their physiological cross-references (i.e. analogous relationships). The significance of this research to the clinical world looks promising, with the advanced techniques and meaningful results attained in the sections above laying the groundwork for future, more comprehensive studies.

6.1 SUMMARY

The novel SAD_{ulf} model is the key deliverable of this research. Insights obtained from model results for ULF IOS may improve the likelihood of early detection of SAD. The presented novel electrical circuit analog of the respiratory system that models small airways disease using two different approaches can be used for enhancing the sensitivity of IOS impedance measurements and lead to improved and timelier diagnosis of asthma in children.

Many of the existing electrical models used today limit their usefulness and compatibility to mono-frequency FOT or traditional IOS research, making the design, development, and testing of a SAD_{ulf} model a new resource for research and eventually improved clinical practice in PFT. The fact that the SAD_{ulf} model is successful in representing lung health or disease from an incomplete patient database, which lacked impedance measurements or any relevant information regarding ULF IOS, demonstrates its power in performance. Focused on providing a potential solution to the SAD detection problem, primarily through an inverse-forward modeling approach,

this research both predicted and validated these lung health and disease inferences within the ultra-low frequency range of IOS.

In summary, outcomes from these modeling efforts show that the inverse modeling technique presented outperforms the presented forward-modeling approach, and in essence self-validated the model by utilizing two very distinct implementations of the modeling algorithms yet still obtaining practically identical results. While the LS analysis performed as expected within the standard 5 to 25 Hz IOS frequency range, we can conclude that the provision of experimental ULF impedance data would drastically improve regression results within this frequency range, particularly for pulmonary system reactance. Furthermore, it was found that this work contribution toward developing a mechano-acoustical to electrical transduction scheme made it feasible to implement an intuitive forward modeling approach using circuit schematic capture and simulation software. The value added from the model transduction and bridge circuit as a respiratory system inhomogeneity index concepts is their potential to facilitate and improve future forward modeling work.

6.2 TECHNICAL ASSUMPTIONS, RISKS, AND CONSTRAINTS

The scope of this research and the results presented in this dissertation can be applied to supplement current IOS capabilities and enhance existing methods for small airways disease diagnosis despite limitations inherent in modeling as a research approach and the specific differences between the SAD_{ulf} model and the human respiratory system [28]. For instance, use of the SAD_{ulf} model is specifically indicated for use with ULF IOS and should only encompass frequency response of the lungs in the range of 0.5 to 5 Hz. Generic and competing respiratory models, or electrical analogs, do exist in the literature and can be applied over a large bandwidth

of frequencies to some extent [38], but caution should be taken and assumptions should not be made when applying these general models to ULF inputs, where data extrapolations often replace actual model outputs. Several of these comprehensive models also tend to exhibit large parameter estimate errors at both extremes of the frequency range, due to signal interference from spontaneous breathing at low frequencies and upper airway shunting effects at high frequencies.

Apart from this, this research may allow machine learning approaches for IOS data classification, which would further augment the precision of results through the application of a validated SAD_{ulf} model. This would be expected to enhance the reliability of classification into four patient groups and corresponding measurements afforded from the used IOS pediatric patient database. For instance, identification of borderline diagnoses due to crossover between two respiratory condition classifications, could be more closely examined for the purpose of improving accuracy, particularly using information from the newly available IOS ULF modeling data.

In addition, the future patient databases could be made more robust by recording parameters associated with input signals, e.g. pressure, flow, and volume measurements; patient-specific breathing cycle information, e.g. breaths/min. and baseline volumes; and of course, respiratory impedance at ULF, which were all lacking from the IOS pediatric patient database used for this research. Furthermore, the inclusion of additional anthropometric data such as physical dimensions of the chest could be added to conduct more thorough mathematical studies and statistical analyses. It is hypothesized that the addition of ULF impedance data, input signal characteristics, and chest size to an IOS data set would result in the definition of discriminative features from electrical models such as SAD_{ulf} model and lead to enabling highly accurate and early diagnoses of small airways diseases.

Finally, the presented ULF IOS pulmonary modeling technique and respiratory impedance results were not examined in their ability to assess therapeutic response under provocation testing, where past studies with competing analog models have found parameter estimates and IOS indices correlate closely with bronchodilator response [37]. Consequently, additional patient records reflecting provocation data were not considered because such modeling is beyond the scope of this research.

6.3 Recommendations for Future Research

To advance techniques for inverse and forward modeling SAD detection in the ULF range, whilst results of regression and circuit simulation indicate that parameter estimate errors and impedance calculation tolerances are indeed acceptable, the effect of tidal breathing should be investigated to determine its effect on modeling performance. Likewise, the recursive combination of inverse and forward modeling into a single dynamic system to methodically reach model convergence to an acceptable error level, say within measurement error, could facilitate individual patient modeling to improve understanding, monitoring, and treatment of SAD through observation of model evolution. Additionally, building a physical circuit of the SAD_{ulf} model for testing per ULF IOS criteria may serve as a validation of the Multisim circuit simulation's respiratory impedance estimates, so as to offer insight of environmental effects on real-world versus virtual results. Finally, use of the SAD_{ulf} to baseline and monitor a subject's lung impedance bias should be investigated as a means to observe the evolution of SAD based on contrasting the relative progress of disease between the subject's lungs.

REFERENCES

[1] J. C. Hogg *et al*., "The Contribution of Small Airway Obstruction to the Pathogenesis of Chronic Obstructive Pulmonary Disease," Physiological Reviews, vol. 97, no. 2, pp. 529–552, Feb. 2017.

[2] Author Unknown (2016). Asthma statistics – United States. American Academy of Allergy Asthma & Immunology. Milwaukee, WI. [Online]. Available: https://www.aaaai.org/about-the-aaaai/newsroom/asthma-statistics.aspx

[3] I. Asher *et al*. (2018, Aug.). The Global Asthma Report. Global Asthma Network. Auckland, New Zealand. [Online]. Available: http://www.globalasthmareport.org

[4] National Asthma Control Program. (2017). Asthma's impact on the nation: Most Recent National Asthma Data. Centers for Disease Control and Prevention. Atlanta, GA. [Online]. Available: https://www.cdc.gov/asthma/reports_publications.htm

[5] C. P. Criée *et al*., "Body plethysmography - Its principles and clinical use," Respiratory Medicine, vol. 105, no. 7, pp. 959–971, Feb. 2011.

[6] Author Unknown (2017). A Brief History of the Spirometer. Jones Medical Instrument Company. Oak Brook, IL. [Online]. Available: www. jonesmedical.com/brief-history-spirometer

[7] S. Bickel *et al*., "Impulse oscillometry: Interpretation and practical applications," Chest, vol. 146, no. 3, pp. 841–847, Sep. 2014.

[8] M. R. Miller *et al*., "Standardization of spirometry," European Respiratory Journal, vol. 26, no. 2, pp. 319–338, 2005.

[9] J. M. D. Mead, "The Lung's 'Quiet Zone'," New England Journal of Medicine, vol. 282, no. 23, pp. 1318–1319, 1970.

[10] N. Beydon *et al*., "An Official American Thoracic Society/European Respiratory Society Statement: Pulmonary Function Testing in Preschool Children," American Journal of Respiratory and Critical Care Medicine, vol. 175, no. 12, pp. 1304–1345, 2007.

[11] H. Maes *et al*., "Estimation of Respiratory Impedance at Low Frequencies During Spontaneous Breathing Using the Forced Oscillation Technique," in 36th Annual International Conference of the IEEE EMBC, Chicago, IL, 2014, pp. 3410-3413.

[12] E. G. Meraz *et al*., "Impulse Oscillometric Features and Respiratory System Models Track Small Airway Function in Children," in Practical Applications in Biomedical Engineering, 1st ed., London, United Kingdom: Intech Open, 2012, ch. 5, pp. 103-140.

[13] H. J. Smith *et al*., "Forced oscillation technique and impulse oscillometry," European Respiratory Monograph, vol. 31, pp. 72–105, Apr. 2005.

[14] A. B. DuBois *et al*., "Oscillation Mechanics of Lungs and Chest in Man," Journal of Applied Physiology, vol. 8, no. 6, pp. 587–594, May 1956.

[15] W. Tomalak *et al*., "Impulse oscillometry vs. body plethysmography in assessing respiratory resistance in children," Pediatric Pulmonology, vol. 41, no. 1, pp. 50–54, 2006.

[16] E. D. Michaelson *et al*., "Pulmonary mechanics by spectral analysis of forced random noise," Journal of Clinical Investigation, vol. 56, no. 5, pp. 1210–1230, Nov. 1975.

[17] H. D. Komarow *et al*., "Impulse oscillometry in the evaluation of diseases of the airways in children," Annals of Allergy, Asthma and Immunology, vol. 106, no. 3, pp. 191–199, 2011.

[18] G. R. Washko, "Diagnostic Imaging in COPD," Semin Respir Crit Care Med, vol. 31, no. 3, pp. 276–285, Jun. 2010.

[19] A. Saltos *et al*., "Comparison of Respiratory Resistance Measurements Made with an Airflow Perturbation Device with Those from Impulse Oscillometry," Journal of Medical Engineering, vol. 2013, no. 165782, pp. 1–11, 2013.

[20] E. Oostveen *et al*., "The forced oscillation technique in clinical practice: Methodology, recommendations and future developments," European Respiratory Journal, vol. 22, no. 6, pp. 1026–1041, 2003.

[21] K. R. Lutchen *et al*., "Importance of Low-Frequency Impedance Data for Reliably Quantifying Parallel Inhomogeneities of Respiratory Mechanics," IEEE Transactions on Biomedical Engineering, vol. 35, no. 6, pp. 472-481, 1988.

[22] Z. Hantos *et al*., "Forced oscillatory impedance of the respiratory system at low frequencies," Journal of Applied Physiology, vol. 60, no. 1, pp. 128-132, 1986.

[23] J. Cao and A. Sabharwal, "Portable Forced Oscillation Device for Point-of-care Pulmonary Function Testing," in 38th Annual International Conference of the IEEE EMBC, Orlando, FL, 2016, pp. 2282-2286.

[24] N. Avila *et al*., "Characterization of Impulse Oscillometric Measures of Respiratory Small Airway Function in Children," Advances in Electrical and Electronic Engineering, vol. 17, no. 1, pp. 54-63, 2019.

[25] E. G. Meraz *et al*., "Reference equations for impulse oscillometric and respiratory system model parameters in Anglo and Hispanic children," Revista Mexicana de Ingenieria Biomedica, vol. 37, no. 1, pp. 1-13, 2016.

[26] A. B. Otis *et al*., "Mechanical Factors in Distribution of Pulmonary Ventilation," Journal of Applied Physiology, vol. 8, no. 4, pp. 427-443, 1956.

[27] M. Schmidt *et al*., "Computer simulation of the measured respiratory impedance in newborn infants and the effect of the measured equipment," Medical Engineering & Physics, vol. 20, pp. 220-228, 1998.

[28] J. Bates, Lung Mechanics An Inverse Modeling Approach. New York: Cambridge University Press, 2009, p. 1-206.

[29] J. Mead, "Contribution of compliance of airways to frequency-dependent behavior of lungs," Journal of Applied Physiology, vol. 26, no. 5, pp. 670-673, 1969.

[30] C. Ionescu and R. de Keyser, "Parametric models for characterizing respiratory input impedance," Journal of Medical Engineering and Technology, vol. 32, no. 4, pp. 315-324, 2008.

[31] B. Klug and H. Bisgaard, "Measurement of Lung Function in Awake 2-4-Year-Old Asthmatic Children During Methacholine Challenge and Acute Asthma: A Comparison of the Impulse Oscillation Technique, the Interrupter Technique, and Transcutaneous Measurement of Oxygen Versus Whole Body Plethysmography," Pediatric Pulmonology, vol. 21, pp. 290-300, 1996.

[32] M. D. Goldman *et al*., "Clinical applications of forced oscillation to assess peripheral airway function," Respiratory Physiology and Neurobiology, vol. 148, pp. 179-194, 2005.

[33] S. Gonem, "Non-invasive Assessment of Small Airway Obstruction in Asthma," Ph.D. dissertation, Dept. of Infection, Immunity, and Inflammation, Univ. of Leicester, England, 2015.

[34] J. Bates, "Assessment of Peripheral Lung Mechanics," Respiratory Physiology and Neurobiology, vol. 163, no. 1-3, pp. 54-63, 2008.

[35] J. G. Eyles and R. L. Pimmel, "Estimating Respiratory Mechanical Parameters in Parallel Compartment Models," IEEE Transactions on Biomedical Engineering, vol. BME-28, no. 4, pp. 331-317, 1981.

[36] J. Glapiński et al., "Analysis of the method for ventilation heterogeneity assessment using the Otis model and forced oscillations," Computer Methods and Programs in Biomedicine, vol. 122, no. 122, pp. 330-340, 2015.

[37] C. Ramos Rocha, "Modeling Impulse Oscillometry Data: Using Augmented-RIC and Extended-RIC Respiratory Impedance Model Parameters to Track Pulmonary Health and Disease," Master's thesis, Dept. of Electrical and Computer Engineering, Univ. of Texas El Paso, Texas, 2011.

[38] K. Lutchen and K. Costa, "Physiological interpretations based on lumped element models fit to respiratory impedance data: Use of forward-inverse modeling," IEEE Transactions on Biomedical Engineering, vol. 37, no. 11, pp. 1076-1086, 1990.

APPENDIX A

Least Squares Approximation Plots of Resistance per Respiratory Condition

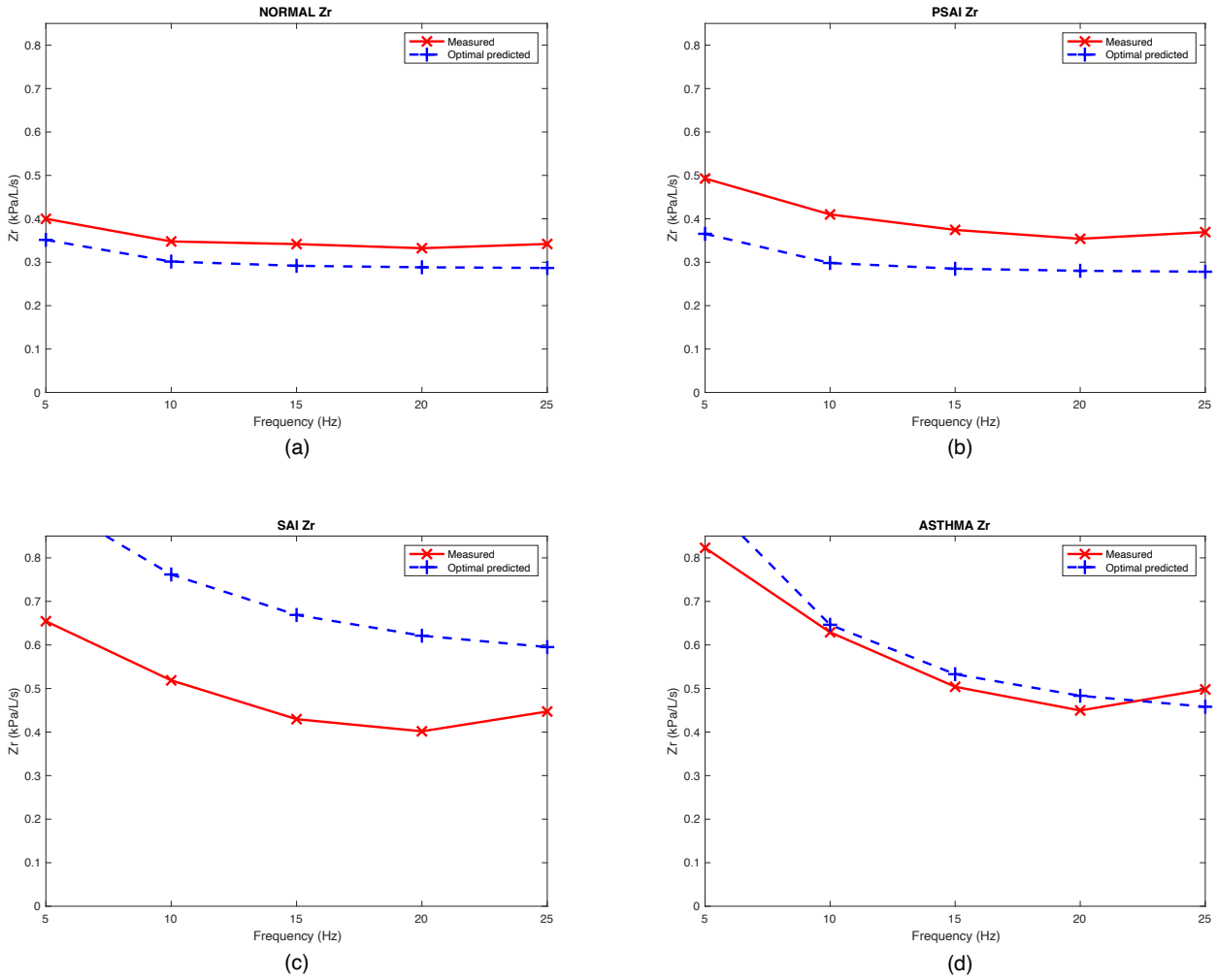

Figure A.1: Least squares regression curves of Resistance (*Zr*) data for (a) Asthma, (b) PSAI, (c) SAI, and (d) Normal conditions per MATLAB parameter optimization algorithm.

APPENDIX B

Least Squares Approximation Plots of Reactance per Respiratory Condition

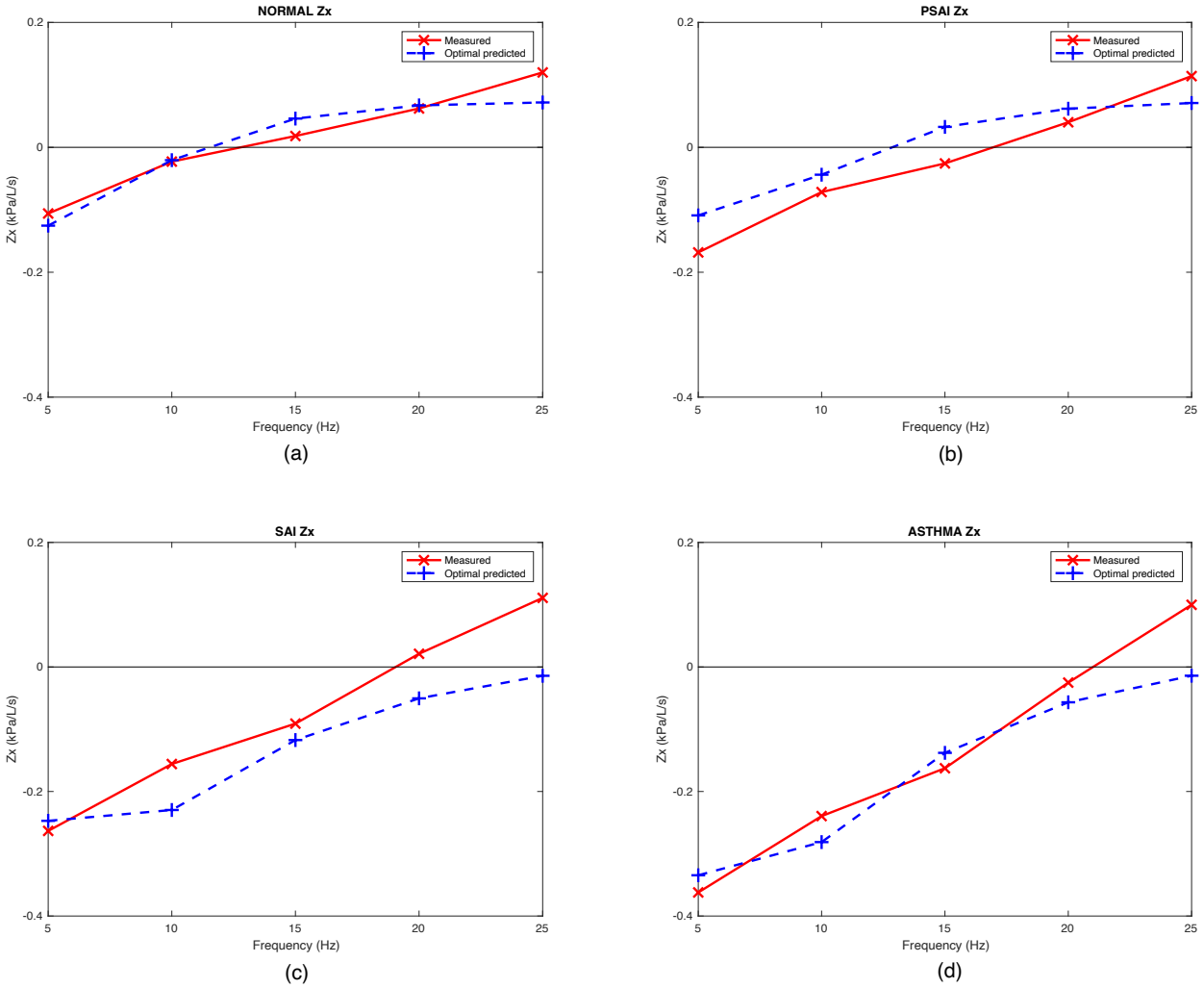

Figure A.2: Least squares regression curves of Reactance (*Zx*) data for (a) Asthma, (b) PSAI, (c) SAI, and (d) Normal conditions per MATLAB parameter optimization algorithm.

CURRICULUM VITA

Christopher Michael Aguilar was born and raised in El Paso, Texas. He received the B.S. degree in electrical engineering in 1998 from the University of Southern California in Los Angeles. In 2003 and 2008, he received the M.S. degree in manufacturing engineering and the Masters of business administration degree, respectively, from the University of Texas at El Paso; where he recently received the Ph.D. degree in electrical engineering (biomedical engineering concentration) in 2020.

He has more than five years of experience in the electronics industry, over 13 years of experience in the medical/healthcare industry, and 25 years in manufacturing. He has also worked in academia and held several appointments as a graduate research assistant, teaching assistant, and lecturer during his tenure. Since 2014, his research interests are associated with medical devices and instrumentation, with an emphasis on mobile health diagnostic equipment, particularly regarding coronary and pulmonary diseases.

Dr. Aguilar is a member of IEEE and Biomedical Engineering Society (BMES), is a certified lean six sigma green belt, and holds a patent for a surgical facemask.